Q. J. R. Meteorol. Soc. (2006), **132**, pp. 1423–1456 doi: 10.1256/qj.05.79

The influence of large convective eddies on the surface-layer turbulence

By S. S. ZILITINKEVICH[1,2]†, J. C. R. HUNT[3], I. N. ESAU[2], A. A. GRACHEV[4], D. P. LALAS[5], E. AKYLAS[6], M. TOMBROU[6], C. W. FAIRALL[7], H. J. S. FERNANDO[8], A. A. BAKLANOV[9] and S. M. JOFFRE[10]

[1]*Division of Atmospheric Sciences, University of Helsinki, Finland*
[2]*Nansen Environmental and Remote Sensing Centre/Bjerknes Centre for Climate Research, Bergen, Norway*
[3]*Department of Space & Climate Physics and Earth Sciences, University College London, UK*
[4]*University of Colorado CIRES/NOAA ETL‡, USA and A. M. Obukhov Institute of Atmospheric Physics, Russian Academy of Sciences, Moscow, Russia*
[5]*National Observatory of Athens, Greece*
[6]*Laboratory of Environmental Physics, University of Athens, Greece*
[7]*NOAA Environmental Technology Laboratory, Boulder, USA*
[8]*Environmental Fluid Dynamics Program, Arizona State University, Tempe, USA*
[9]*Danish Meteorological Institute, Copenhagen, Denmark*
[10]*Finnish Meteorological Institute, Helsinki, Finland*

(Received 9 May 2005; revised 31 October 2005)

SUMMARY

Close to the surface large coherent eddies consisting of plumes and downdraughts cause convergent winds blowing towards the plume axes, which in turn cause wind shears and generation of turbulence. This mechanism strongly enhances the convective heat/mass transfer at the surface and, in contrast to the classical formulation, implies an important role of the surface roughness. In this context we introduce the stability-dependence of the roughness length. The latter is important over very rough surfaces, when the height of the roughness elements becomes comparable with the large-eddy Monin–Obukhov length. A consistent theoretical model covering convective regimes over all types of natural surfaces, from the smooth still sea to the very rough city of Athens, is developed; it is also comprehensively validated against data from measurements at different sites and also through the convective boundary layer. Good correspondence between model results, field observations and large-eddy simulation is achieved over a wide range of surface roughness lengths and convective boundary-layer heights.

KEYWORDS: Convection Heat and mass transfer Minimum friction velocity Semi-organized structures Surface fluxes

1. INTRODUCTION

This paper focuses on the near-surface turbulent mixing and heat/mass transfer with particular attention to the role of large-scale, semi-organized eddies driven by buoyancy forces. In the shear-free convective boundary layer (CBL), where the mean wind velocity is lower than or comparable with typical horizontal velocities in large eddies, the eddies are principally similar to three-dimensional Benard-type cells composed of: narrow uprising plumes (updraughts), wide downdraughts, convergence flows oriented towards the plume base close to the surface, and divergence flows at the CBL upper boundary. Such eddies have been observed in the atmosphere with strong and uniform surface buoyancy flux (e.g. Priestley 1954; Lenschow *et al.* 1980). As follows from perturbation analysis (Elperin *et al.* 2002, 2006) they can result from the convective flow instability, and are closer in nature to almost regular micro-circulations than to real, chaotic turbulence. Observed features of long-lived, CBL-scale convective eddies in calm weather are shown in Fig. 1 based on airborne measurements (Williams and Hacker 1992).

† Corresponding author: Division of Atmospheric Sciences, University of Helsinki, Finland.
e-mail: sergej.zilitinkevich@fmi.fi
‡ Cooperative Institute for Research in the Environmental Sciences/National Oceanic and Atmospheric Administration Environmental Technology Laboratory.

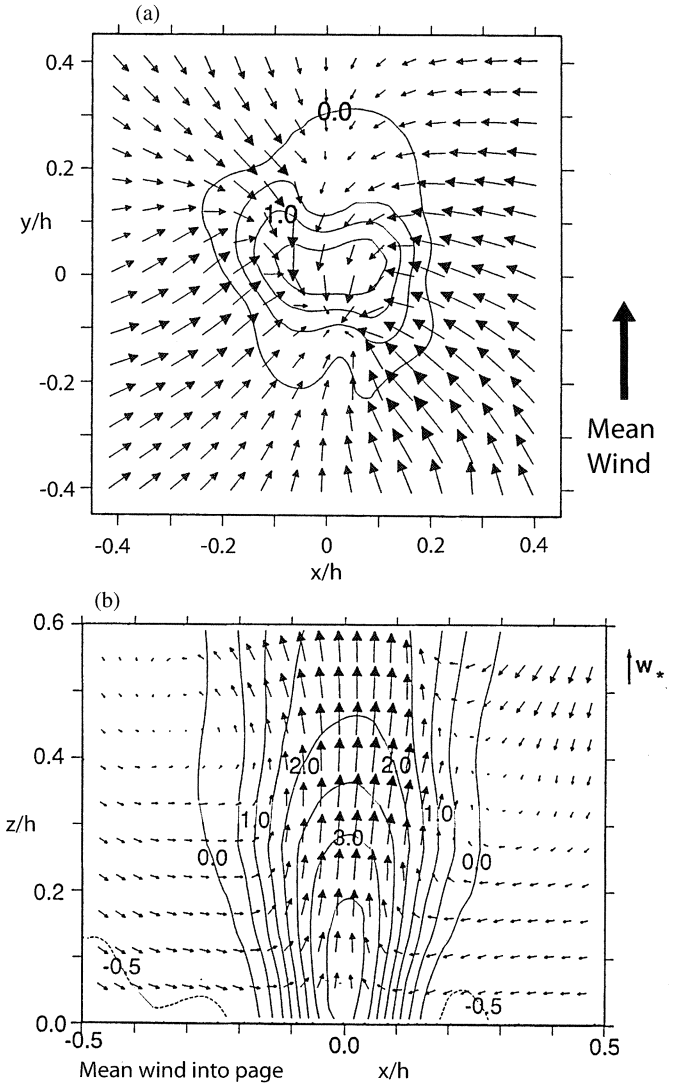

Figure 1. Large convective eddy during a calm sunny day over the Australian desert (after airborne measurements of Williams and Hacker (1992)): (a) horizontal (x, y) cross-section, and (b) vertical (x, z) cross-section. Arrows show the large-eddy velocity field (subtracting the mean wind). Solid lines show the deviations of potential temperature, θ, from its averaged value, $\langle\theta\rangle$. The iso-surface $\theta - \langle\theta\rangle = 0$ marks the side walls of the updraught.

The length- and the velocity-scales characterizing large eddies are the CBL depth, h, and the Deardorff (1970, 1972a) convective velocity:

$$W_* = (F_{bs}h)^{1/3}. \tag{1}$$

Here, $F_{bs} = \beta F_{\theta s} + 0.61 g F_{qs}$ is the surface value of the vertical turbulent flux of buoyancy, b, which includes the temperature flux, $F_{\theta s}$, and the humidity flux, F_{qs}; g is the acceleration due to gravity; $\beta = g/T_0$ is the buoyancy parameter where T_0 is a reference value of absolute temperature. The buoyancy is defined as $b = -g\rho/\rho_0$, where ρ is the air density and ρ_0 is its reference value. The local shearing flows over the surface in the cells generate mechanical turbulence and enhance mixing. Hence, the nature of

the surface-layer turbulence depends on h and also on the surface roughness length, z_{0u}. Traditional local theories overlook this mechanism and underestimate the surface fluxes in strong convection.

The eddy–shear models developed by Schumann (1988) and Sykes *et al.* (1993) suggested how to combine the effects of the convectively generated turbulence, the shear generated turbulence and roughness effects at the surface. Schumann's model (a one-layer model assuming the dominant role of the buoyancy forces throughout the convergence flows) shows reasonably good correspondence with empirical data and data from large-eddy simulation (LES) of CBLs over moderately rough surfaces ($10^4 < h/z_{0u} < 10^5$), but becomes inaccurate in the asymptotic regimes of the low roughness ($h/z_{0u} > 10^6$) and the very high roughness ($h/z_{0u} < 10^3$). Whereas the Sykes *et al.* (1993) model (another one-layer model assuming the dominant role of the large-eddy shears and employing logarithmic profiles in the convergence flows) performs reasonably well over smooth surfaces but is not valid over rough and very rough surfaces. Until recently the above models were considered as contradicting alternatives.

Zilitinkevich *et al.* (1998) developed a more general two-layer model, which accounted both for buoyancy and shear mechanisms, and employed 'log + power law' profiles dependent on z/L_*, where L_* is the large-eddy Monin–Obukhov (henceforth MO) length:

$$L_* = \frac{U_*^3}{F_{bs}}, \tag{2}$$

based on the so-called 'minimum friction velocity' U_* caused by the interaction of the convergence flow and the surface†. In this context, L_* is the depth over which the role of the shear processes becomes negligible. To validate their model, Zilitinkevich *et al.* (1998) used field data, which gave essentially larger values of U_*/W_* than LES data used by Schumann (1988) and Sykes *et al.* (1993).

Akylas *et al.* (2001, 2003) explained that this contradiction is due to the fact that empirical estimates of U_* based on field data are practically always affected by the ambient mean wind. They proposed a special procedure of extracting the ambient wind shear contribution from the measured U_*, and by this means achieved a reasonable correspondence between experimental and LES data. They also made new turbulence measurements in convective regimes over very rough surfaces (the city of Athens and its surroundings) and using these extended our knowledge about U_*/W_* to $h/z_{0u} \sim 10^3$.

Putting together all available LES and observational data, it becomes clear that none of the earlier models applies to the whole range of roughness lengths and CBL heights: $10^2 < h/z_{0u} < 10^9$. In this paper it is shown that the Schumann (1988) model from one side, and the Sykes *et al.* (1993) and Zilitinkevich *et al.* (1998) models from the other side, are valid in certain intervals of h/z_{0u}. In the former model, the turbulent eddies are assumed to be determined by buoyant convection, even very close to the surface; in the latter models, the shear-driven turbulence is considered to be the only dominant factor close to the surface (this is not valid in the case of very high-roughness elements).

A more complete formulation is developed in the present paper. It includes both regimes and, moreover, accounts for the effect of buoyancy on the effective roughness length. This effect, overlooked in all prior models, becomes essential over surfaces with a typical height of roughness elements comparable with the MO length. The proposed new theory agrees with LES and field data over the whole interval of geophysical importance: $10^2 < h/z_{0u} < 10^9$. It makes use of: a new theoretical model of the

† This paper focuses on the convective regimes when the surface buoyancy flux F_{bs} is positive. For convenience, we determine the MO length as positive in these regimes.

stability-dependence of the effective roughness length developed by Zilitinkevich *et al.* (2003); new statistical theory of turbulent eddies in buoyant convection developed by Hunt (1984) and Hunt *et al.* (1988a); and measurements of local profiles in very strong convection by Rao and Narasimha (1996). We also use recent perturbation analyses, plus experiments on turbulent layers with surface heating (Owinoh *et al.* 2005) and with finite height roughness elements (Belcher *et al.* 2003); the former show explicitly how convective eddies affect the momentum of the mean flow, and how the interaction of impinging eddies with large roughness elements affects the profiles.

2. PHYSICAL BACKGROUND

(*a*) *Traditional concepts*

Most theoretical models of surface-layer turbulence are based on Monin and Obukhov (1954) similarity theory. For the dry atmosphere (neglecting the effect of humidity on the density stratification) scaling arguments show that near the surface the turbulence regime is fully determined by the mean values of the near-surface fluxes of momentum, τ_s, and potential temperature, $F_{\theta s}$, and also the buoyancy parameter, β:

$$\tau_s = \rho_0 |\overline{\mathbf{u}'w'}|_{z=0}, \quad F_{\theta s} = \overline{\theta' w'}|_{z=0}, \quad \beta = g/T_0, \tag{3}$$

where z is the height over the surface, $\mathbf{u} = \mathrm{i}u + \mathrm{j}v$ is the horizontal velocity vector (with streamwise, u, and transverse, v, components), w is the vertical velocity and θ is the potential temperature; primes denote turbulent fluctuations, and over-bars denote the ensemble- or time-mean values. By extension, the scales of velocity, potential-temperature, buoyancy and length composed from these parameters are:

$$u_* = (\tau_s/\rho_0)^{1/2}, \quad \theta_* = -F_{\theta s}/u_*, \quad b_* = -F_{bs}/u_*, \quad L = u_*^3/F_{bs} = u_*^2/b_*, \tag{4}$$

where $F_{bs} = \beta F_{\theta s}$ is the near-surface buoyancy flux, and L is the MO length based on the mean-shear-generated friction velocity, u_* (as already mentioned, we define L as positive in unstable stratification). According to the MO theory, the mean vertical gradients of wind velocity and potential temperature are expressed through universal functions of the dimensionless height z/L:

$$\frac{\partial u}{\partial z} = \frac{u_*}{k_u z}\Phi_M\left(\frac{z}{L}\right), \quad \frac{\partial \theta}{\partial z} = \frac{\theta_*}{k_T z}\Phi_H\left(\frac{z}{L}\right), \tag{5}$$

where $k_u \approx 0.4$ and $k_T \approx 0.4$ are the von Kármán constants; $\Phi_M(z/L)$ and $\Phi_H(z/L)$ are empirical universal functions that satisfy the conditions $\Phi_M(0) = 1$ and $\Phi_H(0) = 1$. Integrating Eq. (5) over z and employing roughness lengths z_{0u} for wind and z_{0T} for temperature, to parametrize the flow–surface interaction, the velocity and temperature profiles become:

$$u(z) = k_u^{-1} u_* \{\ln(z/z_{0u}) + \Psi_M(z/L) - \Psi_M(z_{0u}/L)\}, \tag{6a}$$

$$\theta(z) - \theta_s = k_T^{-1}\theta_* \{\ln(z/z_{0T}) + \Psi_H(z/L) - \Psi_H(z_{0T}/L)\}. \tag{6b}$$

Here, subscript s again indicates the value at the surface ($z = 0$); and functions Ψ_M and Ψ_H are the integrals:

$$\Psi_{\{M,H\}}(\xi) = \int \{\Phi_{\{M,H\}}(\xi) - 1\}\xi^{-1}\, \mathrm{d}\xi. \tag{7}$$

Given the roughness parameters, z_{0u} and z_{0T}, and taking $u(z)$, $\theta(z)$ and θ_s from measurements or from a numerical model, Eqs. (4d) and (6a,b) can be solved for u_*, θ_* and L. Then the fluxes of momentum, τ_s, and heat, $F_{Hs} = \rho_0 c_p F_{\theta s}$ (where c_p is the specific heat of air at constant pressure) are immediately found: $\tau_s = \rho_0 u_*^2$, $F_{Hs} = -\rho_0 c_p u_* \theta_*$ (e.g. Monin and Yaglom 1971).

The MO theory and the flux calculation techniques based on this theory show good agreement with experimental data in regimes with sufficiently strong winds. In particular, Eqs. (6a,b) yield well-grounded logarithmic profiles in neutral stratification (when u_* is high or F_{bs} is small, so that $L = u_*^3/F_{bs} > 100$ m).

We focus here on the extreme (but not infrequent) regime of vanishing mean wind speeds, when the friction velocity, u_*, caused by the mean wind shear also vanishes, so that $L \to 0$ and $\theta_* \to \infty$. Then Eqs. (6) become questionable. Indeed, these equations are derived through term-wise integration of Eq. (5) from near the surface ($z = 0$) to an arbitrary height z, employing roughness lengths z_{0u} and z_{0T} to describe the effect that the interactions between flow and surface has on the velocity and temperature profiles, provided they have logarithmic forms over a finite interval. This interval lies above the typical height of roughness elements: $z > h_0$, but below the MO length-scale: $z \ll L$. The ratio h_0/z_{0u} characterizes the surface, and depends on the density and shape of the roughness elements. Its typical value from laboratory experiments using surfaces with the roughness of sand is 25; the same value is applied to the roughness length of urban canopies (e.g. Monin and Yaglom 1971; Baklanov *et al.* 2005). For practical use it is more convenient to characterize natural surfaces by z_{0u} rather than h_0, because operational models deal with databases of z_{0u}. Then, taking $h_0 \approx 25 z_{0u}$, we conclude that the logarithmic-profile interval, $25 z_{0u} < z \ll L$, completely vanishes at $L < 25 z_{0u}$.

Recall that the classical formulation for the velocity and temperature gradients in free convection (Prandtl 1932; Obukhov 1946, 1960; Monin and Obukhov 1954) does not imply any logarithmic intervals:

$$\frac{\partial u}{\partial z} = \frac{C_U u_*^2}{F_{bs}^{1/3} z^{4/3}}, \quad u(z) = u_a - \frac{3 C_U u_*^2}{(F_{bs} z)^{1/3}}, \tag{8a}$$

$$\frac{\partial \theta}{\partial z} = -\frac{C_\Theta F_{\theta s}}{F_{bs}^{1/3} z^{4/3}}, \quad \theta(z) = \theta_a + \frac{3 C_\Theta F_{\theta s}}{(F_{bs} z)^{1/3}}. \tag{8b}$$

Here, $C_U = 1.7$ and $C_\Theta = 1.1$ are dimensionless constants (Kader and Yaglom 1990). The constants of integration designated here by u_a and θ_a are nothing but the mean wind speed and potential temperature in the well-mixed interior of the CBL (sufficiently far from the surface).

In this essentially local theory, the only turbulent velocity-scale is the Prandtl scale:

$$W_c = (F_{bs} z)^{1/3}. \tag{9}$$

An alternative analysis of the turbulence structure, consistent with the above conclusions but based on the statistical theory of inhomogeneous turbulence, without making similarity assumptions, has been developed by Hunt (1984). A model based on dynamics of large eddies impacting on the ground (but ignoring surface stress) yields predictions for the vertical velocity variance, length-scales, spectra and two point correlations that agree well with atmospheric data. This approach is generalized in the present paper to allow for the effects of surface stress very close to the surface.

A heat-transfer model consistent with the above free-convection theory (Malkus 1954; Priestley 1954) is based on the assumption that the turbulent mixing processes

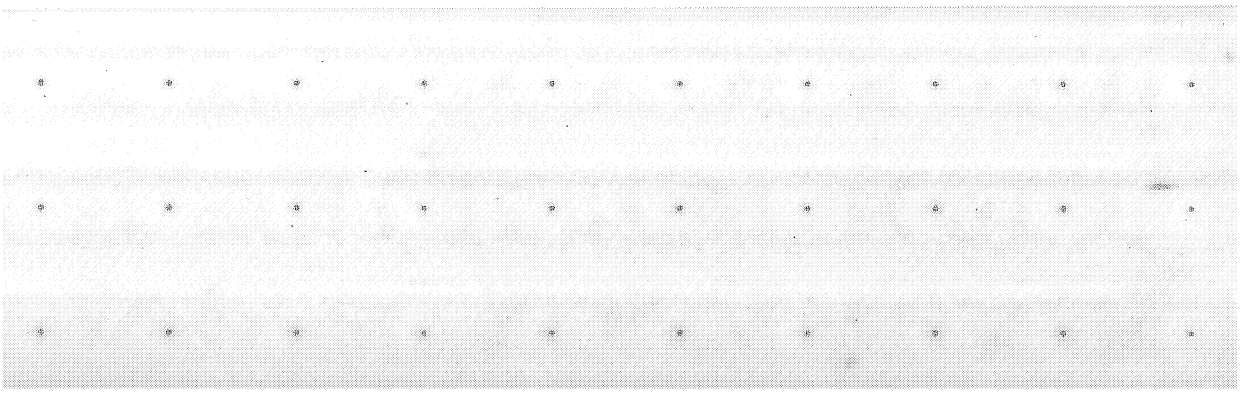

are fully controlled by locally generated convective eddies. Because W_c diminishes toward the surface, the depth of the near-surface viscous sub-layer $\sim\nu/W_c$ (where ν is the molecular viscosity) should be large, so that even high-roughness elements are immersed in this sub-layer. Then the interaction of the flow with roughness elements plays little or no role. In the viscous layer the governing parameters of the temperature profile are $F_{\theta s}$, β, ν, and the molecular heat conductivity, κ. Then, matching the temperature profiles in the viscous layer and in the free-convection layer yields the heat-transfer law:

$$F_{\theta s} = C_{\rm conv}\left(\frac{\beta\kappa}{\rm Pr}\right)^{1/3}\Delta\theta^{4/3}, \tag{10}$$

where $C_{\rm conv}$ is a dimensionless coefficient, ${\rm Pr} = \nu/\kappa$ is the Prandtl number, and $\Delta\theta$ is the temperature difference between the surface and the convective-layer interior.

In engineering applications, Eq. (10) is often presented in terms of the Nusselt and Rayleigh numbers, Nu and Ra, respectively:

$$\mathrm{Nu} = C_{\rm conv}Ra^{1/3}, \quad \text{where} \quad \mathrm{Nu} \equiv \frac{F_{\theta s}h}{\kappa\Delta\theta}, \text{ and } \mathrm{Ra} \equiv \frac{\beta\Delta\theta h^3}{\kappa\nu}. \tag{11}$$

Here h is the depth-scale (in the atmosphere the CBL depth), which effectively drops out from Eq. (11). These models make no allowance for the roughness of the surface.

Equations (10) or (11) and the similar mass-transfer law have been verified in hundreds of laboratory experiments. They are presented in handbooks and recommended for use in atmospheric applications by Deardorff (1972b), Liu *et al.* (1979), Golitsyn (1979), Golitsyn and Grachev (1986), Grachev (1989) and many others, with the conventional value of $C_{\rm conv} = 0.14$. Howard (1990) extended this formulation to include the effect of the mean wind shear. In contrast to this tradition, we demonstrate (see section 5) that this classical law, although it performs reasonably accurately in laboratory experiments†, is absolutely inapplicable to atmospheric CBLs.

An alternative heat-transfer law making some allowance for rough surfaces has been derived from Eq. (8b) by substituting the roughness length, z_{0u}, for z, and the aerodynamic surface temperature, θ_0, for $\theta(z)$:

$$F_{\theta s} = (3C_\Theta)^{-3/2}(\beta z_{0u})^{1/2}\Delta\theta^{3/2}, \quad \Delta\theta \equiv \theta_0 - \theta_a. \tag{12}$$

Here, θ_0 is determined as an notional value of θ obtained through extending the $-1/3$ power law profile down to the level $z = z_{0u}$. Taking the known empirical value of $C_\Theta = 1.1$, the coefficient on the right-hand side (r.h.s.) of Eq. (12) becomes $(3C_\Theta)^{-3/2} \approx 0.2$. This version of Eq. (12) has been recommended for practical use, e.g. by Louis (1979).

Schumann (1988) has derived the same relationship as Eq. (12) accounting for the effect of large eddies. However, in his model the empirical coefficient on the r.h.s. was no longer equal to $(3C_\Theta)^{-3/2}$; instead it was evaluated from LES and happened to be an order of magnitude larger than 0.2.

The above formulations are immediately extended to the wet atmosphere by substituting the virtual potential temperature $\theta_v = \theta + 0.61T_0q$ for θ, where q is the specific humidity. The buoyancy flux $F_{bs} = \beta F_{\theta s} + 0.61gF_{qs}$, and the MO length, L, are modified to include the humidity flux, F_{qs}, or the turbulent humidity-scale, q_*:

$$L = u_*^3/\beta F_{\theta vs} = u_*^2(\beta\theta_* + 0.61gq_*)^{-1}, \quad q_* = -F_{qs}/u_*. \tag{13}$$

† More recently it has been recognized that this law is not quite correct even as applied to laboratory CBLs (see Siggia 1994) and represents only a reasonable first approximation.

Then the MO theory suggests the same formulation for the specific humidity (based on q_*) as Eqs. (5) and (6b) for the potential temperature (based on θ_*). Moreover, empirical estimates of the dimensionless constants in the specific-humidity and the potential-temperature profiles are quite close and usually taken as equal: i.e. $k_q \approx k_T \approx 0.4$ and $C_Q \approx C_\Theta \approx 1.1$, where k_q and C_Q are the 'humidity von Kármán' constant and the constant in humidity gradient formulation analogous to Eq. (8b).

(*b*) *Large eddies: their role in the surface layer and the minimum friction velocity*

Atmospheric measurements and the impacting eddy model (Belcher *et al.* 2003) show that near the surface the r.m.s. of the vertical turbulent velocity varies as $W_c = (F_{bs}z)^{1/3}$. The horizontal turbulent velocities are of the order of the Deardorff scale $W_* = (F_{bs}h)^{1/3}$. The significance of this scaling was realized by Priestley (1959) who first analysed convective turbulence in terms of buoyant plumes (see Hunt *et al.* 2003).

Businger (1973a,b) also recognized the mechanism of large-scale convergence flow patterns as an inherent feature of the convective surface layer. He treated these patterns as internal boundary layers (IBLs) and introduced a concept of the minimum friction velocity, U_*, defined through a scalar averaging: $U_*^4 = \langle (u'w')^2 \rangle + \langle (v'w')^2 \rangle$, where angle brackets designate the time average (or horizontal space average in LES) in contrast to the traditional vector averaging ($u_*^4 = \langle u'w' \rangle^2 + \langle v'w' \rangle^2$) which obviously affords $u_* \to 0$ when the mean wind vanishes. In this conceptual model, U_* depends on the CBL governing parameters: F_{bs}, h, z_{0u}; and the resistance coefficient, defined as U_*/W_*, is a monotonically decreasing function of h/z_{0u}:

$$U_*/W_* = \Phi_*(h/z_{0u}). \tag{14}$$

Wyngaard and Cote (1974) and Panofsky *et al.* (1977) revealed the same physical mechanism in their analysis of the horizontal velocity variances, σ_u^2 and σ_v^2, in the convective surface layer. They discovered that σ_u^2 and σ_v^2 are basically proportional to the Deardorff velocity-scale:

$$\sigma_u^2 \equiv \overline{u'^2} = C_{uu}W_*^2, \quad \sigma_v^2 \equiv \overline{v'^2} = C_{vv}W_*^2, \tag{15}$$

whereas the vertical velocity variance, σ_w^2, behaves in reasonable agreement with the Prandtl, Obukhov, and MO similarity theories:

$$\sigma_w^2 \equiv \overline{w'^2} = C_{ww1}W_c^2, \tag{16a}$$

or, in the presence of shear:

$$\sigma_w^2 = C_{ww1}W_c^2 + C_{ww2}u_*^2. \tag{16b}$$

The coefficients $C_{ww1} = 1.1$ and $C_{ww2} = 1.7$ were determined quite accurately from field measurement (Lenschow *et al.* 1980) and LES (Moeng and Wyngaard 1989), whereas the coefficients C_{uu} and C_{vv} in Eq. (15) varied between 0.2 and 0.6 (Yaglom 1994; Hibberd and Sawford 1994).

Since the length-scale of vertical fluctuations is proportional to z (Hunt 1984), combining these results shows that the eddy viscosity K_M, heat conductivity K_H, and water vapour diffusivity K_D in the IBL (all three proportional to $\sigma_w z$) have two different limiting forms, namely:

$$K_{\{M,H,D\}} \sim U_* z \text{ at } z \ll L_* \quad \text{where shear turbulence dominates,} \tag{17a}$$

$$K_{\{M,H,D\}} \sim W_* h^{-1/3} z^{4/3} \text{ at } z \geqslant L_* \quad \text{where convective turbulence dominates.} \tag{17b}$$

These expressions are consistent with the measurements of Rao and Narasimha (1996) taken in very strong convective conditions in India.

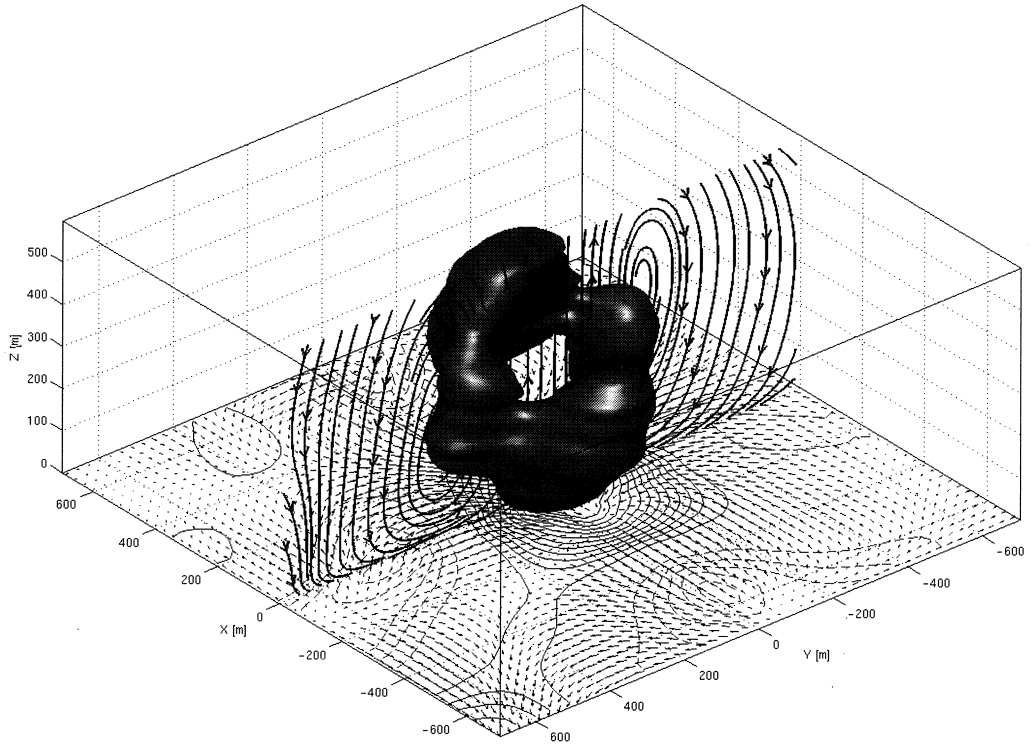

Figure 2. A large-eddy simulation 'portrait' of the first characteristic eddy (that is the most energetic one) in the shear-free convective boundary layer. This eddy is retrieved from run 31a (see Table 2). Data for this analysis were sampled every ~30 s over the 15-minute run time (a total of 28 samples) starting from the 12th hour of the simulation. Horizontal velocity (arrows) and vertical velocity (contours) within the surface layer (from 18 to 50 m) are shown in the horizontal (x, y) plane. The maximum horizontal velocity (the longest arrow) is 2.8 m s^{-1}. Solid contours in the horizontal plane mark updraughts, starting with 0.14 m s^{-1}, then 0.18 m s^{-1}, and subsequently stepping by 0.06 m s^{-1} up to 0.84 m s^{-1}. The maximum updraught velocity is 1.2 m s^{-1}. Dashed contours mark downdraughts from -0.16 m s^{-1} to -0.8 m s^{-1} with -0.08 m s^{-1} steps. Bold curves with arrows in the vertical (y, z) plane show streamlines; their asymmetry is probably caused by gradual growth of the convective cells during the sampling period, so that the flow is not statistically stationary. The central torus visualizes the iso-surface of the modulus of the eddy-induced vorticity at 65% of its maximal value.

3. LARGE-EDDY BOUNDARY-LAYER MODEL

(*a*) *Internal boundary layer: basic features and vertical profiles*

Following earlier models of Schumann (1988), Sykes *et al.* (1993) and Zilitinkevich *et al.* (1998), we assume that large eddies are characterized by the length-scale, h, and the velocity-scale, W_* (see Eq. (1)), and live much longer than the CBL overturning time, $h/W_* \sim 10^3$ s (although shorter than the time-scale of the evolution of the mean flow). Accordingly, the large-scale convergence flow field near the surface is treated as a quasi-steady IBL, in which the smaller-scale turbulence is in local equilibrium.

As shown in Fig. 1, this conceptual model is consistent with observational evidence (for more information see: Williams and Hacker 1992, 1993; Williams *et al.* 1996). It is also strongly supported by our LES (see subsection 2(d)). Figure 2 based on a LES shows a topological structure of a statistically significant CBL-scale convective eddy—what it looks like after filtering the turbulent noise. It reveals principally the same type of

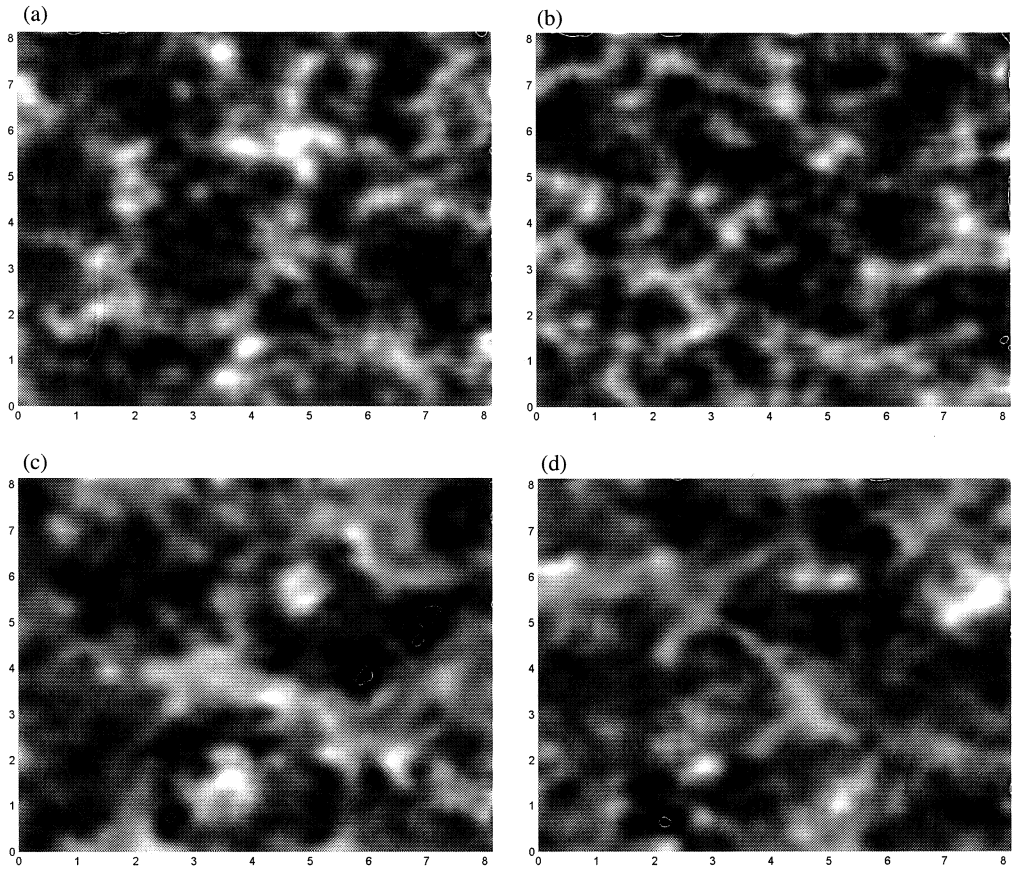

Figure 3. Snapshots of the distribution of potential-temperature, θ, fluctuations, $\theta(x, y, z) - \langle\theta\rangle$, within different convective boundary layers (CBLs): (a) in the lower part, over a very smooth surface (large eddy simulation (LES) run 2, see Table 1); (b) in the lower part, over a very rough surface (LES run 30); (c) and (d) are as (a) and (b), respectively, but in the upper part of the CBL. Brighter areas correspond to larger positive fluctuations. The domain sizes are given in kilometres.

eddy circulation as in Fig. 1, and clearly demonstrates that the near-surface large-eddy motion (shown by arrows) is indeed an IBL type of flow.

The eddy in Fig. 2 is obtained by retrieving statistically the most significant components of the velocity field using a proper orthogonal decomposition (POD) technique. Its mathematical background is given by e.g. Berkooz *et al.* (1993). It is essentially the well-known principal-component analysis but conducted in spectral space, which allows the extraction of moving and changing structures at the peak of their evolution, when the structures contain the maximum energy. Moin and Moser (1989) first applied the POD technique to retrieve coherent structures in a simulated turbulent flow. They also worked out a phase-recovery method to present eddies in physical space. Wilson (1996) and Esau (2003) have used the POD technique to retrieve coherent structures from LES data reproducing atmospheric boundary layers. The eddy structure in Fig. 2 exhibits quite good correspondence, not only with the airborne measurement data in Fig. 1, but also with directly simulated instant eddies as depicted in Fig. 3.

In accordance with the above evidence, the principal length-scales characterizing the gross features of the shear-free CBL are:

- CBL depth h;
- IBL depth h_I;
- The 'constant-flux' layer depth, estimated as one tenth of the IBL depth;
- The depth h_{SL} of the 'surface layer' (defined as the layer with pronounced vertical increments in the convective wind speed and virtual potential temperature or buoyancy) known to be about an order of magnitude larger than the large-eddy MO lengths L_* (see Eq. (2)); so $h_{SL} \sim 10L_*$;
- The depth h_{SSL} of the 'surface shear layer' (SSL)† estimated as one tenth of L_*; so $h_{SSL} \sim 10^{-1}L_*$, $L_* \sim 10^{-3}h$;
- The typical height of roughness elements, h_0, related to the roughness length for momentum, z_{0u}, as $h_0 \sim 25z_{0u}$;
- The horizontal-scale X of the IBL, estimated as approximately $1/3$ of the distance between plume structures; so $X \sim h/3$.

Of these scales, h is the largest (in the atmosphere of order 10^3 m). The depth of the surface layer is much smaller: $h_{SL} \sim 10L_* = 10(U_*/W_*)^3 h \sim 10^{-2}h$. As shown below, the IBL depth (see Eq. (29)) is only an order of magnitude smaller than h (then $h_I \sim 10^{-1}h \sim 10^2 L_*$, which is why the constant-flux layer and surface layer coincide). The fact that the surface layer occupies only the lower 10% of the IBL simplifies further analysis. It allows modelling the near-surface part of the IBL through the MO similarity theory (Eqs. (3)–(7)) or, alternatively, through the eddy-viscosity/conductivity/diffusivity model (Eqs. (17a,b)) with the IBL-flow velocity U, and large-eddy friction velocity U_*, substituted for the ordinary wind velocity u, and friction velocity u_*.

In its principal features, the IBL is similar to a stagnation-point boundary layer near $x = 0$ (defined as the midway point between two vertically rising plumes) where the downdraught impinges at the surface, and the large-scale velocity above the IBL, U_I, behaves as $U_I \sim W_* x/X$. However, following Priestley (1959), near the plume (at $x = X$) the flow above the IBL is entrained into the plume and accelerates so that $U_I \sim (X - x)^\gamma$. Here $\gamma = 0$ for a two-dimensional line plume and $\gamma = -1$ for a three-dimensional plume (Turner 1973). Thus there are significant horizontal pressure gradients proportional to $U_I \partial U_I/\partial x$ in the convergent flows. The surface shear causes an additional perturbation, $\tilde{u}$, to the IBL flow velocity, hence $U = U_I + \tilde{u}$. Note that the shear has negligible effect near the stagnation (downdraught) region: $\tilde{u} = 0$ at $x = 0$. The pressure gradient is balanced by the acceleration above the IBL (as in Hunt *et al.* 1988a,b). Then, in the main part of the IBL (excluding the surface layer where $z \leqslant 10L_*$) to leading order in a linearized theory the velocity perturbation is given by:

$$U_I(x)\frac{\partial \tilde{u}}{\partial x} \cong \frac{\partial \tau}{\partial z}. \tag{18}$$

In an approximate analysis developed below, the average value $\langle U_I \rangle \sim W_*$ is taken for the advective velocity over the length-scale X.

For $z > 10^{-1}L_*$ the perturbation shear stress, τ, is generated primarily by the local convective-wind shear interacting with the turbulence generated by convection. By contrast, Sykes *et al.* (1993) only considered shear-generated turbulence in the IBL.

† The SSL is the lower part of the surface layer, in which the shear-generated turbulence dominates. Above the SSL buoyancy-generated turbulence dominates. These two regimes change at the threshold height $\sim C_* L_*$, where $C_* \sim 10^{-1}$ (e.g. Monin and Yaglom 1971; Kader and Yaglom 1990).

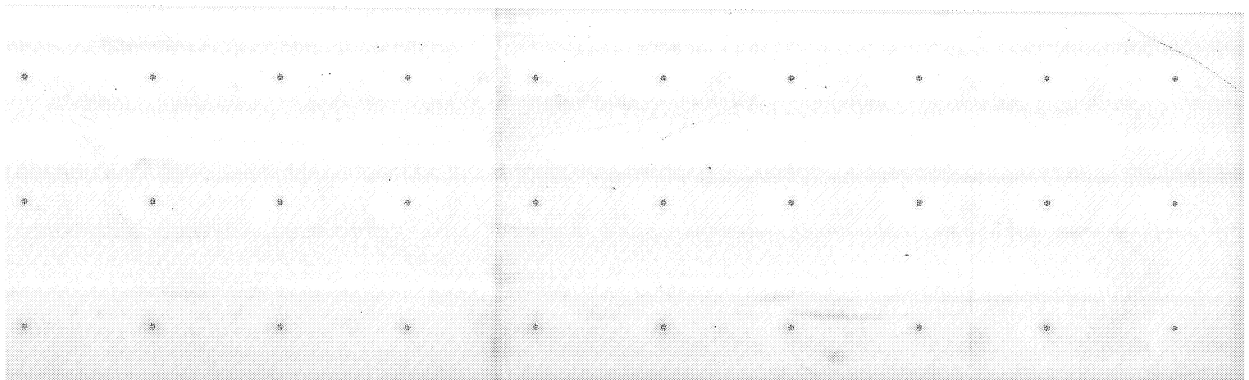

In the surface layer, where $z \leqslant 10L_*$, the 'mean' profiles in the IBL are determined by the approximately depth-constant local turbulent fluxes:

$$\tau = U_*^2 = K_{\mathrm{M}}\frac{\partial U}{\partial z}, \quad F_\theta = F_{\theta\mathrm{s}} = -K_{\mathrm{H}}\frac{\partial \theta}{\partial z}, \quad F_q = F_{q\mathrm{s}} = -K_D\frac{\partial q}{\partial z}, \tag{19}$$

(and the perturbation analysis is not relevant). Recall that these fluxes are horizontally variable, and our analysis aims at the estimation of there area-averaged (aggregated) values.

Equations (17a,b) are combined with a single interpolation formula:

$$K_{\{\mathrm{M,H,D}\}} = z\left\{k_{\{u,T,q\}}U_* + \frac{W_*}{C_{\{U,\Theta,Q\}}}\left(\frac{z}{h}\right)^{1/3}\right\}, \tag{20}$$

where C_U and C_Θ are the same dimensionless constant as in Eqs. (8a,b), C_Q and k_q are the same type of constants as C_Θ and k_T but in the humidity profile equations similar to Eqs. (6b) and (8b).

To exclude the problem of the heat/mass transfer within the roughness layer, we formulate the boundary conditions in terms of the aerodynamic surface potential temperature, θ_0, and specific humidity, q_0:

$$U = 0, \quad \theta = \theta_0, \quad q = q_0 \quad \text{at } z = z_{0u}, \tag{21}$$

where θ_0 and q_0 are defined by extending the self-similar surface-layer profiles $\theta(z)$ and $q(z)$ down to the level $z = z_{0u}$, where z_{0u} is the roughness length for momentum†.

The solution to Eqs. (19)–(21) for the IBL 'mean velocity' is:

$$U = \frac{U_*}{k_u}\left\{\ln\frac{z}{z_{0u}} - 3\ln\frac{1 + (k_uC_U)^{-1}(z/L_*)^{1/3}}{1 + (k_uC_U)^{-1}(z_{0u}/L_*)^{1/3}}\right\}. \tag{22}$$

This formulation is consistent with the Owinoh *et al.* (2005) analysis and computation of the surface layer when the heat flux varies in space and time, as in this case. In the IBL above the surface shear layer, where $h_{\mathrm{I}} > z \gg L_*$, Eq. (22) shows that U varies in proportion to $(z/L_*)^{-1/3}$, and at $z \sim 10L_*$ tends to a depth-constant value which can be identified with U_{I} (parametrically dependent on the horizontal coordinate x). As already mentioned, the roughness length for momentum, z_{0u}, is usually taken to be proportional to the typical height of obstacles: $z_{0u} \sim 0.04h_0$. Corrections to this definition for high roughness and strong buoyancy flux, and also for very low roughness, are introduced later.

For surfaces with low levels of roughness ($z_{0u} \ll L_*$; typically $z_{0u} < 0.03$ m) the logarithmic term is dominant near the surface. In this regime the asymptotic form of the IBL wind profile at $z/L_* \gg 1$ and the upper limit of the 'mean velocity' are:

$$U \approx \frac{U_*}{k_u}\left\{\ln\frac{L_*}{z_{0u}} + 3\ln(k_uC_U) + \frac{3}{k_uC_U}\left(\frac{z_{0u}}{L_*}\right)^{1/3} - 3k_uC_U\left(\frac{z}{L_*}\right)^{-1/3}\right\}, \tag{23a}$$

$$U \to U_{\mathrm{I}} = \frac{U_*}{k_u}\left\{\ln\frac{L_*}{z_{0u}} + 3\ln(k_uC_U)\right\}. \tag{23b}$$

In Eq. (23b), the term $\sim(z_{0u}/L_*)^{1/3}$ is neglected as $z_{0u} \ll L_*$.

† The differences $\theta_{\mathrm{s}} - \theta_0$ and $q_{\mathrm{s}} - q_0$ between the actual $(\theta_{\mathrm{s}}, q_{\mathrm{s}})$ and the aerodynamic (θ_0, q_0) values are controlled by specific physical processes at the flow–surface interface (e.g. Beljaars and Holtslag 1991; Zilitinkevich *et al.* 2001). Their determination represents an independent problem beyond the scope of the present paper.

However, over rough surfaces (with $z_{0u} \geqslant L_*/10$; typically $z_{0u} \geqslant 1$ m, as in urban areas) Eq. (22) shows that the 'mean velocity' has another asymptotic form and tends to another limit:

$$U \approx 3C_U U_* \left\{ \left(\frac{z_{0u}}{L_*} \right)^{-1/3} - \left(\frac{z}{L_*} \right)^{-1/3} \right\}, \tag{24a}$$

$$U \to U_{\mathrm{I}} = 3C_U U_* \left(\frac{z_{0u}}{L_*} \right)^{-1/3}. \tag{24b}$$

In both Eqs. (23) and (24) the perturbation velocity $\tilde{u} = U - U_{\mathrm{I}}$ in the upper part of the surface layer behaves as $-3C_U U_* (z/L_*)^{-1/3}$. As already mentioned, U_{I} is proportional to the Deardorff velocity-scale: $\langle U_{\mathrm{I}} \rangle = C_{\mathrm{a}} W_*$, where C_{a} is an empirical dimensionless constant of order unity.

A similar analysis for θ and q in the surface layer yields the solution similar to Eq. (22):

$$\left\{ \frac{k_T U_* (\theta - \theta_0)}{-F_{\theta \mathrm{s}}}, \frac{k_q U_* (q - q_0)}{-F_{q\mathrm{s}}} \right\} = \ln \frac{z}{z_{0u}} - 3 \ln \frac{1 + (k_{\{T,q\}} C_{\{\Theta,Q\}})^{-1} (z/L_*)^{1/3}}{1 + (k_{\{T,q\}} C_{\{\Theta,Q\}})^{-1} (z_{0u}/L_*)^{1/3}}, \tag{25}$$

which also has two alternative asymptotes corresponding to comparatively smooth surfaces:

$$\left\{ \frac{k_T U_* (\theta - \theta_0)}{-F_{\theta \mathrm{s}}}, \frac{k_q U_* (q - q_0)}{-F_q} \right\}$$

$$\approx \ln \frac{L_*}{z_{0u}} + 3 \ln \left\{ k_{\{T,q\}} C_{\{\Theta Q\}} + \frac{3}{k_{\{T,q\}} C_{\{\Theta,Q\}}} \left(\frac{z_{0u}}{L_*} \right)^{1/3} - 3 k_{\{T,q\}} C_{\{\Theta,Q\}} \left(\frac{z}{L_*} \right)^{-1/3} \right\}, \tag{26a}$$

$$\left\{ \frac{k_T U_* \Delta\theta}{F_{\theta \mathrm{s}}}, \frac{k_q U_* \Delta q}{F_q} \right\} = \ln \frac{L_*}{z_{0u}} + 3 \ln (k_{\{T,q\}} C_{\{\Theta,Q\}}); \tag{26b}$$

and very rough surfaces:

$$\left\{ \frac{U_* (\theta - \theta_0)}{-F_{\theta \mathrm{s}}}, \frac{U_* (q - q_0)}{-F_q} \right\} \approx 3C_{\{\Theta,Q\}} \left\{ \left(\frac{z_{0u}}{L_*} \right)^{-1/3} - \left(\frac{z}{L_*} \right)^{-1/3} \right\}, \tag{27a}$$

$$\left\{ \frac{U_* \Delta\theta}{F_{\theta \mathrm{s}}}, \frac{U_* \Delta q}{F_q} \right\} = 3C_{\{\Theta,Q\}} \left(\frac{z_{0u}}{L_*} \right)^{-1/3}; \tag{27b}$$

where $\Delta\theta = \theta_0 - \theta_{\mathrm{a}}$ and $\Delta q = q_0 - q_{\mathrm{a}}$ are the increments in θ and q across the IBL; θ_{a} and q_{a} are the values characteristic of the CBL interior. In the problem under consideration $\Delta\theta$ and Δq are given parameters.

In the bulk of the IBL the velocity perturbation $\tilde{u}(x, z) = U - U_{\mathrm{I}}$ is determined by Eq. (18), and similarly for the temperature and humidity perturbations $\theta - \theta_{\mathrm{I}}$ and $q - q_{\mathrm{I}}$. Using the expression (17b) for K_{M}, it follows that:

$$U_{\mathrm{I}}(x) \frac{\partial \tilde{u}}{\partial x} \sim \frac{\partial}{\partial z} \left(\frac{W_* z^{4/3}}{h^{1/3}} \frac{\partial \tilde{u}}{\partial z} \right). \tag{28}$$

The approximate solution to this equation, taking U_I as a constant, shows that $\tilde{u}$ matches smoothly with the surface-layer solution given by Eq. (22) as $z/h_I \to 0$ and $z/L_* \to \infty$.

The IBL thickness $h_I(x)$ increases from $x = 0$ (the stagnation zone) in the same way as a plume thickness grows in a convective boundary layer, namely:

$$W_* \frac{dh_I}{dx} \sim 0.24 W_c(z = h_I) = 0.24 W_* \left(\frac{h_I}{h}\right)^{1/3},$$

$$\text{so that } h_I \sim 10^{-1} \frac{x^{3/2}}{h^{1/2}} \text{ and } \langle h_I \rangle \sim 10^{-1} h. \tag{29}$$

Here, the Prandtl velocity-scale W_c (see Eq. (9)) characterizes the vertical velocity variance $\sigma_w(z = h_I)$, and the coefficient 0.24 is taken after tank experiments by Deardorff *et al.* (1980).

The velocity perturbation $\tilde{u}$ decays rapidly with z, so that the velocity in the IBL matches smoothly with U_I above the IBL. In this analysis $U_a \sim W_*$ is assumed to be constant along the IBL. But in some circumstances, such as where the bottom surface has low thermal conductivity (relative to the fluid) and where the heat flux emanates from the solid (rather than from radiation at the surface) the surface flux varies between the stagnation point $x = 0$ and the initiation of the plume $x = X$ (Hunt *et al.* 2003); and this affects the IBL. Therefore the empirical constants in Eqs. (22)–(27), although designated by the same symbols (k_u, k_T, k_q, C_*, C_U, C_Θ, C_Q) as in Eqs. (5)–(8), could differ from standard micrometeorological values. Accordingly all constants in the resistance and heat/mass-transfer laws derived below are determined through direct empirical validation of the proposed formulations.

Experimental data analysed by Kader and Yaglom (1990) show that the matching height, z_*, between the logarithmic and the $-1/3$ power law profiles is about an order of magnitude smaller than the MO length L. This observation supports Eq. (20), which gives $z_*/L \sim (k_{\{u,T,q\}} C_{\{U,\Theta,Q\}})^3 < 0.3$. Thus, in the problem under consideration it is guaranteed that $z_* < 0.3 L_* \sim 2 \times 10^{-4} h$. If $h \sim 1500$ m, then $z_* \sim 0.3$ m.

As already mentioned, the log-profile interval over rough surfaces is also limited from below—by the typical height of roughness elements, $h_0 \sim 25 z_{0u}$. In other words, the logarithmic profiles exist only in the height interval:

$$25 z_{0u} < z < z_* \sim 0.3 (U_*/W_*)^3 h \sim 3 \times 10^{-4} h. \tag{30}$$

Therefore for $h/z_{0u} < 10^5$ the logarithmic interval disappears, so that the mean profiles are of the free-convection type throughout the surface layer, while at $h/z_{0u} > 10^5$ the free-convection layer is separated from the surface by the logarithmic layer.

It follows that the Schumann (1988) one-layer free-convection model, justified when $h/z_{0u} < 10^5$, complements rather than contradicts the two-layer models of Zilitinkevich *et al.* (1998) and Akylas *et al.* (2001) and the one-layer model of Sykes *et al.* (1993), justified when $h/z_{0u} > 10^5$.

(*b*) *Low-roughness surfaces*

The potential-temperature and specific-humidity profiles in the convective sheared surface layer are characterized by practically identical empirical constants: $k_q = k_T$ and $C_Q = C_\Theta$ (e.g. Kader and Yaglom 1990). Then, taking $U_I = C_a W_*$, Eqs. (23b) and (26b)

become:

$$\frac{k_u C_a W_*}{U_*} = \ln\frac{L_*}{z_{0u}} + 3\ln(k_u C_U), \quad k_T C_\Theta U_* \left\{\frac{\Delta\theta}{F_{\theta s}}, \frac{\Delta q}{F_{qs}}, \frac{\Delta b}{F_{bs}}\right\} = \ln\frac{L_*}{z_{0u}} + 3\ln(k_T C_\Theta), \tag{31}$$

where $\Delta b = \beta\Delta\theta + 0.61 g \Delta q$ is the buoyancy increment across the IBL†.

The constant C_a, as well as the other constants in Eq. (31) that differ from usual micrometeorological estimates because of horizontal heterogeneity of the IBL, are to be determined empirically. To avoid confusion, in further analysis we employ alternative notations for new constants.

Recalling that $L_*/h = (U_*/W_*)^3$, the first Eq. (31) becomes:

$$\frac{W_*}{U_*} = \frac{1}{C_{U1}}\left(\ln\frac{h}{z_{0u}} - 3\ln\frac{W_*}{U_*} + C_{U4}\right), \tag{32a}$$

$$\text{or } \frac{W_*}{U_*} \approx \frac{1}{C_{U1}}\left(\ln\frac{h}{z_{0u}} - C_{U0}\right). \tag{32b}$$

Here, C_{U1} and C_{U4} substitute for the combinations $(k_u C_U)^{-1}$ and $3(k_u C_U)^{-1}\ln(k_u C_U)$, respectively. In the approximate Eq. (32b), C_{U0} is defined as:

$$C_{U0} = -C_{U4} + [\text{mean value of } 3\ln(W_*/U_*) \text{ in the interval } 10^5 < h/z_{0u} < 10^9]. \tag{33}$$

Then, using Eq. (32b) to express the slowly varying term $\ln(W_*/U_*)$ on the r.h.s. of Eq. (32a), and designating $C_{U2} = 3\ln C_{U1} + C_{U4}$, gives a convenient approximation:

$$\frac{U_*}{W_*} = C_{U1}\left(\ln\frac{h/z_{0u}}{\{\ln(h/z_{0u}) - C_{U0}\}^3} + C_{U2}\right)^{-1}, \tag{34}$$

where C_{U0}, C_{U1} and C_{U2} are new dimensionless constants.

Finally, using Eq. (32b) to express $\ln(W_*/U_*)$ and Eq. (34) to express W_*/U_*, the second Eq. (31) gives:

$$\frac{F_{\theta s}}{W_*\Delta\theta} = \frac{F_{qs}}{W_*\Delta q} = \frac{W_*^2}{(\beta\Delta\theta + 0.61 g\Delta q)h}$$

$$= C_1\left(\ln\frac{h/z_{0u}}{\{\ln(h/z_{0u}) - C_{U0}\}^3} + C_{U2}\right)^{-1}\left(\ln\frac{h/z_{0u}}{\{\ln(h/z_{0u}) - C_{U0}\}^3} + C_2\right)^{-1}, \tag{35}$$

where C_1 and C_2 are additional new dimensionless constants. As seen from the derivation, C_1 substitutes $k_T C_\Theta (k_u C_U)^{-1}$ and C_2 substitutes $3\ln\{k_T C_\Theta (k_u C_U)^{-1}\}$. Equations (34)–(35) comprise the resistance law and the heat, mass and buoyancy-transfer laws for the low-roughness surfaces.

(c) *Very rough surfaces*

As demonstrated in subsection 3(a), in the convective surface layer over very rough surfaces ($h/z_{0u} < 10^5$) the turbulence of purely convective origin dominates throughout the surface layer and controls the flow–obstacle interaction. The mean profiles do not include logarithmic mechanical-turbulence intervals, so that the physical meaning of

† The assumptions that $k_q = k_T$ and $C_Q = C_\Theta$ are not essential; if future higher-quality data reveal essential differences between the above coefficients, the only alteration to the analysis given in sections 3(b) to (d) will be to consider $F_{\theta s}(W_*\Delta\theta)^{-1}$ and $F_{qs}(W_*\Delta q)^{-1}$ separately.

the roughness length changes. Clearly, the free-convection formulation for the eddy viscosity, $K_M = C_U^{-1} F_{bs}^{1/3} z^{4/3}$, consistent with Eq. (20), becomes inapplicable in the roughness layer where the turbulent length-scale is no longer proportional to the distance from the surface, z. Instead it could be taken proportional to the typical height of roughness elements, h_0, which in turn is proportional to momentum roughness length in neutral stratification, z_{0u}. Because the energy production is basically due to the buoyancy forces, a reasonable scaling estimate of the eddy viscosity in the roughness layer is $K_M \sim F_{bs}^{1/3} h_0^{4/3} \sim F_{bs}^{1/3} z_{0u}^{4/3}$.

Interpolating between the above two formulas ($K_M \propto z^{4/3}$ and $K_M \propto z_{0u}^{4/3}$) yields $K_M = C_U^{-1} F_{bs}^{1/3} (z + \Phi_0 z_{0u})^{4/3}$, where $\Phi_0 \sim h_0/z_{0u}$ is a dimensionless coefficient much larger than unity. Then the near-surface mean velocity profile becomes

$$u(z) = \frac{3C_U u_*^2}{F_{bs}^{1/3}} \left(\frac{1}{z_0^{1/3}} - \frac{1}{z^{1/3}} \right), \text{ which gives the limit } u_a = \frac{3C_U u_*^2}{W_*} \left(\frac{h}{z_0} \right)^{1/3}, \quad (36)$$

where $z_0 = \Phi_0 z_{0u}$ is an effective roughness length, and u_a is the mean wind speed sufficiently far from the surface, cf. Eq. (8a).

Equation (36) is consistent with Eq. (8a), the only difference being that z_0 replaces z_{0u}. Grachev *et al.* (1997) compared the velocity profile similar to Eq. (36) with observational data, and concluded that the 'free-convection roughness length' (that is z_0 in Eq. (36)) is indeed essentially larger than the usual roughness length, z_{0u}, deduced from the logarithmic wind profiles in neutral stratification. The effect of the buoyancy forces on z_0 is considered in subsection 3(d).

Another inherent feature of the very rough surface regime is the displacement effect of high-roughness elements. Belcher *et al.* (2003) considered a canopy of obstacles with height h_0, spacing X_0 and typical diameter D_0, and investigated how the airflows pass between as well as above the obstacles. As the downdraught impacts on the canopy and drives a horizontal flow through it, most of the flow leaves the canopy over a distance of order X_0^2/D_0. If this is less than the length of the large eddy, h, it means that only a small proportion of the flow travels through the canopy, i.e. for $z < h_0$, $U \ll U_I$. Therefore, the mean flow and turbulent eddies are effectively displaced by a distance $d \sim h_0$ as occurs in unstratified logarithmic layers. The convective eddies do not penetrate the porous canopy because of the blocking (or 'sheltering') effect of the shear layer over the roughness element (Hunt and Durbin 1999; Belcher *et al.* 2003). Therefore the mean velocity profile above the roughness elements is determined by Eq. (36) with z replaced by $z - d$. However, when the IBL depth, h_I, is much larger than the displacement height, d, then the above correction, although important as concerns the near-surface wind, temperature and humidity profiles, does not affect the resistance and heat/mass-transfer laws.

Accounting for possible differences between z_{0u} and $z_0 = \Phi_0 z_{0u}$, Eqs. (24b) and (27b) yield the resistance law:

$$\frac{U_*}{W_*} = C_{U3} \left(\frac{z_0}{h} \right)^{1/6}, \quad (37)$$

where C_{U3} is an empirical constant, which substitutes the combinations $C_a^{1/2} (3C_U)^{-1/2}$; and the heat, mass and buoyancy-transfer laws:

$$\frac{F_{\theta s}}{W_* \Delta\theta} = \frac{F_{qs}}{W_* \Delta q} = \frac{W_*^2}{(\beta \Delta\theta + 0.61 g \Delta q) h} = C_3 \left(\frac{z_0}{h} \right)^{1/3}, \quad (38)$$

where C_3 is one more constant, which substitutes the combination $(3C_\Theta)^{-1}$.

Schumann (1988) derived the same equations but did not distinguish between z_{0u} and z_0. He also obtained empirical estimates of C_{U3} and C_3 from the LES of Schmidt and Schumann (1989).

(*d*) *The effect of buoyancy on the effective roughness length*

In some situations, e.g. in urban areas, the roughness is large enough to penetrate into the inner layer and at the same time the buoyancy flux is sufficiently large for local convective plumes to be generated between the roughness elements. These plumes have typical vertical velocities $w_{*0} \sim (F_{bs} z_0)^{1/3}$. As these plumes with typical diameter $3z_{0u}$ are bent over by the 'convective wind' above the roughness elements, they break up over a vertical distance of order $z_{0u}(w_{*0}/u_*)$ and distort the mean flow (e.g. Coelho and Hunt 1989).Thereby they increase the effective height of the roughness elements by a distance of the order of $z_{0u}(z_{0u}/L)^{1/3}$.

This reasoning is consistent with the scaling analysis given by Zilitinkevich *et al.* (2003). They assumed that the effective roughness length for momentum, z_0, is proportional to the turbulent length-scale within the canopy of obstacles, determined as the ratio of the eddy viscosity-scale to the friction velocity: $z_0 = C_{0u} K_{\mathrm{M}}(h_0)/u_*$. In neutral stratification $K_{\mathrm{M}}(h_0) = k u_* h_0$; then taking $k = 0.4$ and $C_{0u} = 0.1$, the above z_0 coincides with the usual roughness length: $z_0 = C_{0u} k h_0 = \frac{1}{25} h_0 = z_{0u}$. In unstable stratification, K_{M} is given by Eq. (20); then $K_{\mathrm{M}}(h_0) = k h_0 \{k u_* + C_U^{-1}(h_0/L)^{1/3}\}$, and z_0 becomes:

$$\frac{z_0}{z_{0u}} = \Phi_0\left(\frac{z_{0u}}{L}\right) = 1 + C_{0C}\left(\frac{z_{0u}}{L}\right)^{1/3}, \tag{39}$$

where C_{0C} is an empirical constant (its reference value following on from the above scaling arguments is $C_{0C} = (k^{4/3} C_{0u}^{1/3} C_U)^{-1}$).

In shear-free convection we replace L in Eq. (39) by L_*, use the identity $z_{0u}/L_* = (z_{0u}/h)(W_*/U_*)^3$, and substitute W_*/U_* from Eq. (37) to obtain:

$$\frac{z_0}{z_{0u}} = 1 + C_{0C}\left(\frac{z_{0u}}{h}\right)^{1/3} \frac{W_*}{U_*} = 1 + \frac{C_{0C}}{C_{U3}}\left(\frac{z_{0u}}{h}\right)^{1/6}\left(\frac{z_0}{z_{0u}}\right)^{-1/6} \approx 1 + C_{00}\left(\frac{z_{0u}}{h}\right)^{1/7}. \tag{40}$$

The approximate expression on the r.h.s. of Eq. (40) is nothing but linear interpolation between the two asymptotic solutions: $z_0/z_{0u} \approx 1$ when the 'correction term' $C_{0C}(z_{0u}/h)^{1/3} W_*/U_*$ is small compared to unity, and $z_0/z_{0u} \approx (C_{0C}/C_{U3})^{6/7} (z_{0u}/h)^{1/7}$ when this term is large. Here, C_{00} is a dimensionless constant to be determined empirically. The second asymptotic solution suggests its reference value: $C_{00} = (C_{0C}/C_{U3})^{6/7}$. Using this approximation, Eqs. (37) and (38) become:

$$\frac{U_*}{W_*} = C_{U3}\left\{\frac{z_{0u}}{h} + C_{00}\left(\frac{z_{0u}}{h}\right)^{8/7}\right\}^{1/6}, \tag{41}$$

$$\frac{F_{\theta \mathrm{s}}}{W_* \Delta\theta} = \frac{F_{q\mathrm{s}}}{W_* \Delta q} = \frac{W_*^2}{(\beta \Delta\theta + 0.61 g \Delta q) h} = C_3\left\{\frac{z_{0u}}{h} + C_{00}\left(\frac{z_{0u}}{h}\right)^{8/7}\right\}^{1/3}. \tag{42}$$

Equations (34) and (35) for low-roughness surfaces, and Eqs. (41) and (42) for very rough surfaces express the Deardorff convective velocity-scale, $W_* = (F_{bs} h)^{1/3}$, the temperature and humidity fluxes at the surface, $F_{\theta \mathrm{s}}$ and $F_{q\mathrm{s}}$, and the minimum friction velocity, U_*, through the CBL external parameters: $\Delta\theta$, Δq, h and z_{0u}.

4. VERIFICATION OF THE MODEL

(*a*) *Field data*

The theory developed in section 3 is compared with data from experiments over a wide range of natural surfaces including land and sea. The marine data used here were collected by the National Oceanic and Atmospheric Administration (NOAA) Environmental Technology Laboratory in the Pacific Ocean aboard the R/V *Moana Wave* for three cruise legs during the TOGA COARE programme in 1992–1993 and on the Scripps Institute Floating Instrument Platform (R/P *FLIP*) during SCOPE in September 1993. Descriptions of the TOGA COARE and SCOPE can be found in Fairall *et al.* (1996a,b,c), Grachev and Fairall (1997), Grachev *et al.* (1997, 1998), and Zilitinkevich *et al.* (1998, 2001). In the TOGA COARE, measurements were carried out in the tropical warm-pool area of the western Pacific Ocean. The ship was positioned at the centre of the intensive flux array (2°S, 156°E; see Webster and Lukas (1990)) for a total of 70 days of measurements. She usually operated in a 'drift' mode, which means that wind speed measurements were relatively unaffected by errors induced by the mean motion of the ship. During SCOPE, R/P *FLIP* was moored about 15 km north-west of the north-west point of San Clemente Island (off southern California) with good open ocean exposure for north-west winds. Identical seagoing flux systems were used in these experiments, and a detailed description can be found in Fairall *et al.* (1997). The instruments were deployed at the end of a boom 20 m in length, 15 and 11 m above the sea surface for the TOGA COARE and SCOPE, respectively. Sonic anemometer/thermometers and high-speed infrared hygrometers were used to measure turbulent fluxes. Data include 50-minute averaged observations of covariance and inertial-dissipation estimates of the turbulent fluxes of momentum, sensible and latent heat, mean meteorological variables, radiation fluxes, and the CBL height. Several data-quality indicators have been applied to the original atmospheric datasets. Data have been edited for unfavourable relative wind directions, mean wind vector tilt, a manoeuvre of the ship during the record, contamination of the turbulence data by the ship's plume, precipitation, and salt contamination. The sea surface temperature was determined from measurements by floating thermistor at 5 cm depth, with corrections for the cool skin effect. A conventional aspirated temperature/relative-humidity sensor and an infrared hygrometer were used to determine mean temperature and humidity.

Our data collected over land come from five field campaigns described below. The BOREX-95 experiment was performed by Risø National Laboratory over a flat, homogeneous surface near the Borris site in the western part of Denmark in July 1995 (Mikkelsen *et al.* 1996; Grachev *et al.* 1998). A sonic anemometer/thermometer (Solent type) was used to make turbulent measurements of stress and sensible-heat flux at the reference height $z = 7$ m above the surface. The CBL depth, $h \approx 600$ to 900 m, was determined from radiosonde measurements. The measured heat flux and air temperature show a normal diurnal cycle associated with a deep, daytime, well-mixed CBL and a stable nocturnal boundary layer.

The first Phoenix Air Flow Experiment (PAFEX-1) was conducted in the Phoenix metropolitan area (Arizona) during January and February 1998 (Grachev *et al.* 1999). The measurement site was a small field surrounded by trees (10 to 15 m in height) and separately standing business buildings (>10 m high) located in the central part of the valley approximately 9 km north-west of downtown Phoenix. Turbulent measurements of sensible-heat and momentum fluxes were made by a standard ATI fast-response sonic anemometer/thermometer (27 Hz sampling rate) which was mounted on a mast at a fixed height of 10 m above the surface. For fluxes and turbulence statistics 30-minute

and 1 h averaging times were used. The direct eddy-correlation method was used for the momentum and sensible-heat flux calculations. In addition to turbulence measurements, a portable tethered 9 m^3 balloon (AIR-TSB-9) was used for vertical profiling, with two tethersondes (TMT-5A-SP) attached to the tetherline at distances of 7 and 14 m below the balloon. Each tethersonde measured the temperature, relative humidity, pressure, wind speed (cup anemometers) and wind direction.

Three other datasets from different sites with high values of the surface roughness in the greater Attiki peninsula area of Greece are used (Akylas *et al.* 2003). The National Observatory of Athens (NOA) is located near the Athens city centre on the top of a distinct hill. Marousi (hereafter MAR) is a suburban area in the northern outskirts of the city and lies on a gentle slope. Datasets for MAR and NOA were acquired during an earlier experimental campaign (Batcharova and Gryning 1998) undertaken during August and September 1994. Measurements of the three velocity components u, v and w, and the virtual temperature, θ_v, were taken by Kaijo-Denki DAT/TR-61B sonic anemometers with a sampling frequency of 10 Hz, at 15 m above ground level. The semi-rural suburban site of Pikermi (hereafter PIK) is located far from the built area of Athens at the foot of Penteli Mountain. The measurements here were made on a small hilltop, which is surrounded by higher terrain. The measurement campaign at PIK was conducted from 15 February to 8 June 1999 by NOA in the framework of EU Project SFINCS (Surface Fluxes in Climate System). Measurements of u, v, w and θ_v were taken using a CSAT3 (Cambell Scientific Anemometer Sonic Thermometer) with a sampling frequency of 8 Hz at 18.8 m above ground level. A number of radiosonde measurements were also performed at PIK from 28 May to 7 June, at various time intervals. Additionally, 0000 and 1200 UTC radiosondes from the Elliniko airport of Athens were provided by the Hellenic National Meteorological Service for the whole period of both experimental campaigns.

Data from the above experiments were analysed, and the runs exhibiting strong unstable stratification with wind velocities below 1 m s^{-1} were selected as representative of the shear-free convection regime. The surface roughness length with respect to wind, z_{0u}, is calculated by extending the traditional formulation to conditions of strong convection, with due regard for the gustiness corrections to the mean wind profile, where the contribution from gusts is scaled with the Deardorff velocity W_* (Grachev *et al.* 1998).

The selected data are used to determine the minimum friction velocity U_* (from measured absolute values of the momentum flux), the resistance coefficient U_*/W_*, and the aerodynamic heat and mass-transfer coefficients $F_{\theta s}(W_*\Delta\theta)^{-1}$ and $F_{qs}(W_*\Delta q)^{-1}$.

Processing of field data from TOGA COARE, SCOPE, BOREX-95, PAFEX-1 and three Greek datasets, included extraction of the contribution from the mean wind shear to U_* using the technique developed by Akylas *et al.* (2003; their Eq. (10) with subsequent iterations). Similar extraction of the ambient mean wind contribution was applied to the calculation of the sensible- and latent-heat fluxes and the MO length.

(*b*) *LES data*

(i) *Convective boundary layer in a LES.* The shear-free convection in typical atmospheric CBLs is a relatively simple case to deal with in a LES. In this case, energetic motions are of very large scale and almost isotropic. The former assures adequate resolution of energy-carrying fluctuations at relatively coarse meshes; the latter implies that the simplest eddy-viscosity closure for the subgrid turbulence correctly parametrizes the energy dissipation at the smallest grid-scale (see e.g. Smagorinsky 1993).

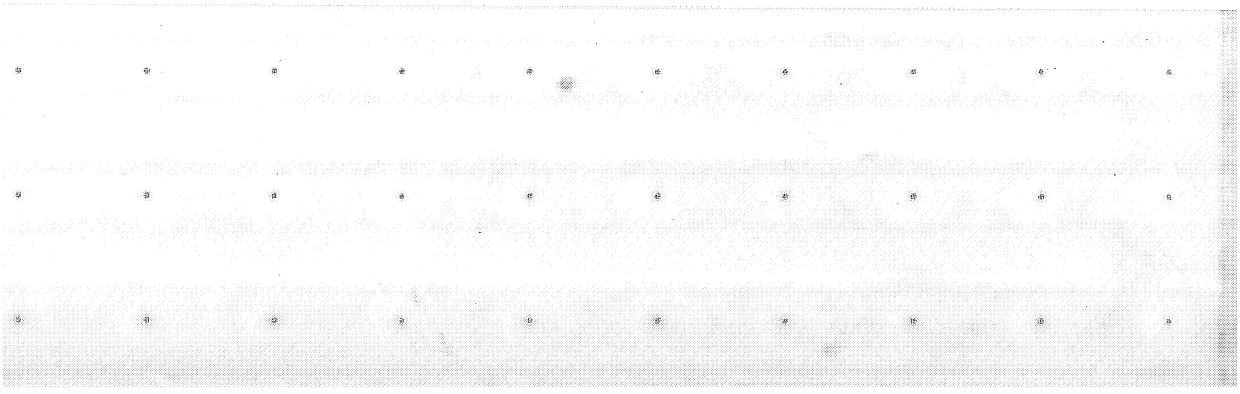

There were several intercomparison studies of the LES of CBLs at different resolution and with different turbulence closure schemes (Nieuwstadt *et al.* 1993; Moeng *et al.* 1996; Fedorovich *et al.* 2004). They reveal excellent agreement, at least in the CBL core, between different LESs for all resolutions down to 40^3 grid nodes. The differences in numerical schemes and turbulence closures resulted in only marginal deviations between LES results—much smaller than the scatter in observational data.

Two layers in the LES domain, namely the SSL and the capping inversion layer (or top of the CBL), are difficult to resolve properly. Indeed, the SSL depth $h_{\mathrm{SSL}} \sim 10^{-3}h$ is very small; hence to resolve this layer, LES must have more than 10^9 grid nodes, which is not yet feasible. To avoid problems with computing of the heat-transfer immediately at the surface, the majority of LESs, including the present one, apply a prescribed temperature flux rather than the air–surface temperature difference. If needed, this latter difference could be calculated diagnostically using one or other assumption about the temperature profile below the first model level. The resolution required to resolve the capping inversion is not so fine. Rampanelli and Zardi (2004) analysed data collected west of Trento, Italy, and reported that the thickness of the inversion in well-developed CBLs is typically a few hundred metres with the potential-temperature gradient $\beta^{-1}N^2 \sim 0.01$ K m^{-1}. Then, according to Canuto and Minotti (1993), fluctuations in the inversion layer are resolved properly at the resolution $\Delta = (5/6 \cdot E/2)^{1/2}\pi N^{-1} \approx 100$ m, where E is the mean turbulent kinetic energy at the top of the mixed layer. Sorbjan (1996) and later Stevens and Bretherton (1999) indicated that a LES of the CBL is generally sensitive to the resolution within the inversion layer, but, when the inversion is properly resolved, the simulated turbulence in the bulk of the CBL becomes remarkably insensitive to the LES resolution.

(ii) *New LES code and data.* The above discussion set up a formal framework for a new LES database, which has been produced using the advanced LES code LESNIC (Large Eddy Simulation Nansen Centre Improved Code, see Esau (2004)). LESNIC employs the dynamic-mixed subgrid model (DMM, Vreman *et al.* 1994) as well as a set of improved numerical schemes; in particular, a fully conservative second order finite-difference advection scheme (Morinishi *et al.* 1998), fourth order Runge–Kutta time advancement scheme and pressure correction scheme (Armfield and Street 1999). LESNIC has been favourably compared with other state-of-the-art LES codes in two intercomparison experiments: for CBLs (Fedorovich *et al.* 2004) and for stable boundary layers (Beare *et al.* 2006).

The DMM is a favourable subgrid model. It has a rigorous mathematical basis and has been found consistent with data from the atmospheric measurement campaign HATS (Horizontal Array Turbulence Study; Sullivan *et al.* 2003). It assures correct energy dissipation, good correlations between the parametrized and true turbulent fluxes (Liu, S. *et al.* 1994) and optimal approximation of the dissipation spectrum (Langford and Moser 1999). Finally, it dynamically restricts the energy cascade in response to increasing anisotropy of the flow in the surface layer. This property allows accurate simulation of the sheared, stratified layers without special tuning of the model parameters. Recall that ad hoc parameter tuning has been used in all earlier LESs (e.g. Sullivan *et al.* 1994).

Table 1 summarizes external (input) and internal (output) parameters of LES runs used in the present paper. These are 50 runs with a resolution of 64^3. The physical resolution is variable; except for the runs with the largest surface roughness, it was adequate to resolve the energetic fluctuations within the CBL core and in the capping inversion. The LES domain is characterized by the following aspect ratio:

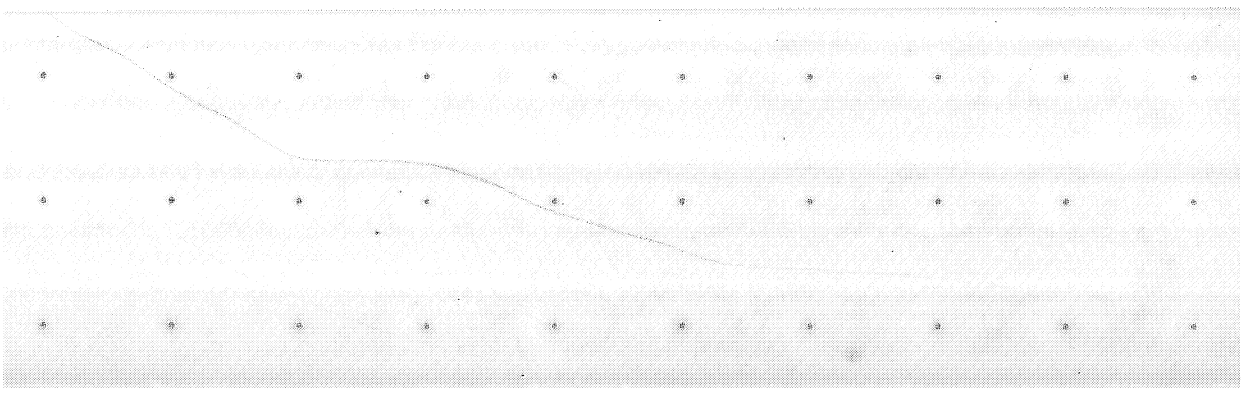

TABLE 1. EXTERNAL AND INTERNAL (CALCULATED) PARAMETERS OF LES

Run	Domain size (km) $Lx \times Ly \times Lz$	$F_{bs} \times 10^4$ (K m^{2}s^{-3})	z_{0u} (m)	N (s^{-1})	Latitude (deg)	U_* (m s^{-1})	W_* (m s^{-1})	$\Delta\theta$ (K)	H (m)
1	6.4 × 6.4 × 2.5	33.3	0.00005	0.0184	45	0.06	1.51	16.1	1035
2	8.0 × 8.0 × 3.5	66.7	0.00005	0.0184	45	0.07	2.12	16.2	1449
3	6.4 × 6.4 × 2.5	33.3	0.0005	0.0184	45	0.07	1.51	7.4	1035
4	8.0 × 8.0 × 3.5	66.7	0.0005	0.0184	45	0.10	2.13	7.4	1449
5	6.4 × 6.4 × 2.5	33.3	0.0001	0.0184	45	0.06	1.51	12.7	1035
6	8.0 × 8.0 × 3.5	66.7	0.0001	0.0184	45	0.08	2.13	12.8	1449
7	8.0 × 8.0 × 3.5	66.7	0.001	0.0184	45	0.12	2.13	5.9	1449
8	6.4 × 6.4 × 2.5	33.3	0.003	0.0184	45	0.10	1.51	3.4	1035
9	4.0 × 4.0 × 1.5	3.3	0.01	0.0184	45	0.03	0.69	4.8	340
10	4.0 × 4.0 × 1.5	16.7	0.01	0.0184	45	0.11	1.05	2.3	691
11	6.4 × 6.4 × 2.5	33.3	0.01	0.0184	45	0.13	1.51	2.6	1035
12	8.0 × 8.0 × 3.5	66.7	0.01	0.0184	45	0.14	2.12	2.7	1449
13	9.6 × 9.6 × 4.0	100	0.01	0.0184	45	0.19	2.58	2.7	1719
14	4.0 × 4.0 × 1.5	3.3	0.1	0.0184	45	0.05	0.48	1.0	440
15	4.0 × 4.0 × 1.5	16.7	0.1	0.0184	45	0.14	1.05	1.0	691
16	8.0 × 8.0 × 3.5	66.7	0.1	0.0184	45	0.24	2.12	1.2	1449
17	9.6 × 9.6 × 4.0	100	0.1	0.0184	45	0.27	2.58	1.2	1719
18	4.5 × 4.5 × 2.0	3.3	1.0	0.0184	45	0.07	0.48	0.2	328
19	6.4 × 6.4 × 2.0	16.7	1.0	0.0184	45	0.21	1.01	0.4	734
20	6.4 × 6.4 × 2.5	33.3	1.0	0.0184	45	0.23	1.51	0.4	1035
21	8.0 × 8.0 × 3.5	66.7	1.0	0.0184	45	0.41	2.12	0.5	1449
22	9.6 × 9.6 × 4.0	100	1.0	0.0184	45	0.60	2.58	0.5	1719
23	6.4 × 6.4 × 2.5	3.3	2.0	0.0184	45	0.10	0.48	0.2	332
24	4.0 × 4.0 × 1.5	16.7	2.0	0.0184	45	0.26	1.02	0.2	645
25	6.4 × 6.4 × 2.5	33.3	2.0	0.0184	45	0.27	1.51	0.3	1035
26	8.0 × 8.0 × 3.5	66.7	2.0	0.0184	45	0.36	2.12	0.4	1449
27	8.0 × 8.0 × 3.5	66.7	3.0	0.0184	45	0.65	2.12	0.3	1449
28	8.0 × 8.0 × 3.0	33.3	5.0	0.0184	45	0.46	1.50	0.1	1008
29	8.0 × 8.0 × 3.5	66.7	5.0	0.0184	45	0.56	2.13	0.2	1449
30	8.0 × 8.0 × 3.5	100	5.0	0.0184	45	0.62	2.58	0.3	1723
31	3.6 × 3.6 × 1.2	33.3	1.0	0.0302	45	0.11	1.11	0.3	413
32	9.0 × 9.0 × 3.0	100	0.05	0.0259	70	0.25	2.28	1.6	1195
33	9.0 × 9.0 × 3.0	166.7	0.05	0.0259	70	0.30	2.94	1.7	1523
34	15.0 × 15.0 × 5.0	266.7	0.05	0.0259	70	0.39	3.75	1.7	1992
35	4.5 × 4.5 × 1.5	50	0.05	0.0336	70	0.15	1.49	1.5	668
36	5.0 × 5.0 × 1.0	16.7	0.05	0.0349	70	0.16	0.84	1.4	352
37	4.5 × 4.5 × 1.5	50	0.05	0.0398	70	0.14	1.42	1.5	574
38	2.1 × 2.1 × 0.7	6.7	0.05	0.0440	70	0.04	0.50	1.2	191
39	2.1 × 2.1 × 0.7	16.7	0.05	0.0440	70	0.08	0.78	1.3	290
40	3.0 × 3.0 × 1.0	50	0.05	0.0520	70	0.14	1.29	1.4	430
41	15.0 × 15.0 × 5.0	33.3	0.05	0.0142	70	0.13	1.66	1.4	1367
42	7.5 × 7.5 × 2.5	33.3	0.05	0.0203	70	0.14	1.45	1.5	918
43	7.5 × 7.5 × 2.5	33.3	0.05	0.0285	70	0.11	1.32	1.4	684
44	5.0 × 5.0 × 1.5	33.3	0.05	0.0300	70	0.15	1.28	1.4	621
45	4.5 × 4.5 × 1.5	33.3	0.05	0.0342	70	0.12	1.21	1.4	527
46	3.6 × 3.6 × 1.2	33.3	0.05	0.0428	70	0.11	1.12	1.4	422
47	3.6 × 3.6 × 1.2	33.3	0.05	0.0485	70	0.11	1.09	1.3	384
48	2.7 × 2.7 × 0.9	33.3	0.05	0.0569	70	0.10	1.02	1.4	316
49	2.4 × 2.4 × 0.8	33.3	0.05	0.0599	70	0.10	1.00	1.4	306
50	1.8 × 1.8 × 0.6	33.3	0.05	0.0713	70	0.09	0.95	1.3	258

Shown are 60-minute averaged values of U_*, $\Delta\theta$ and h calculated for the 5th hour of each run. Longer averaging periods would be unreasonable, as simulated CBLs continue to grow at the rate $\propto t^{1/2}$. See text for details of parameters.

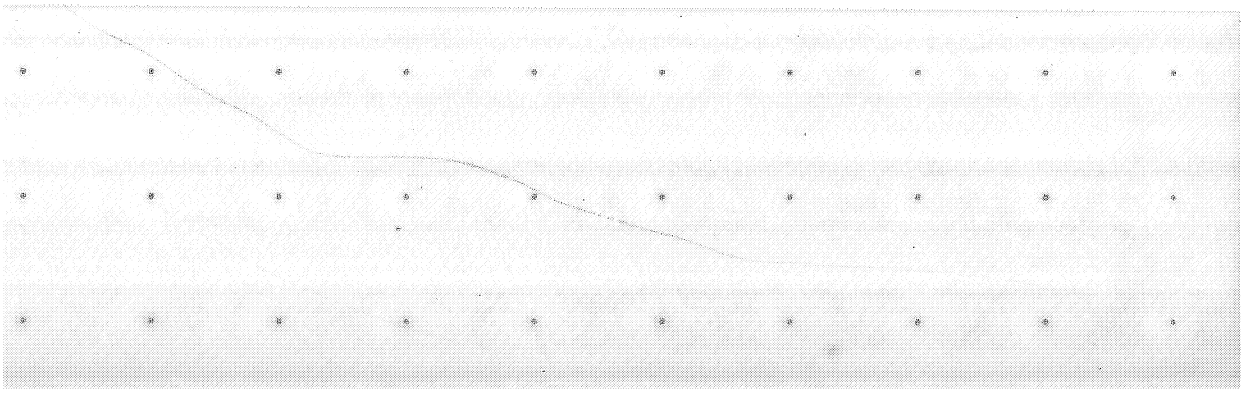

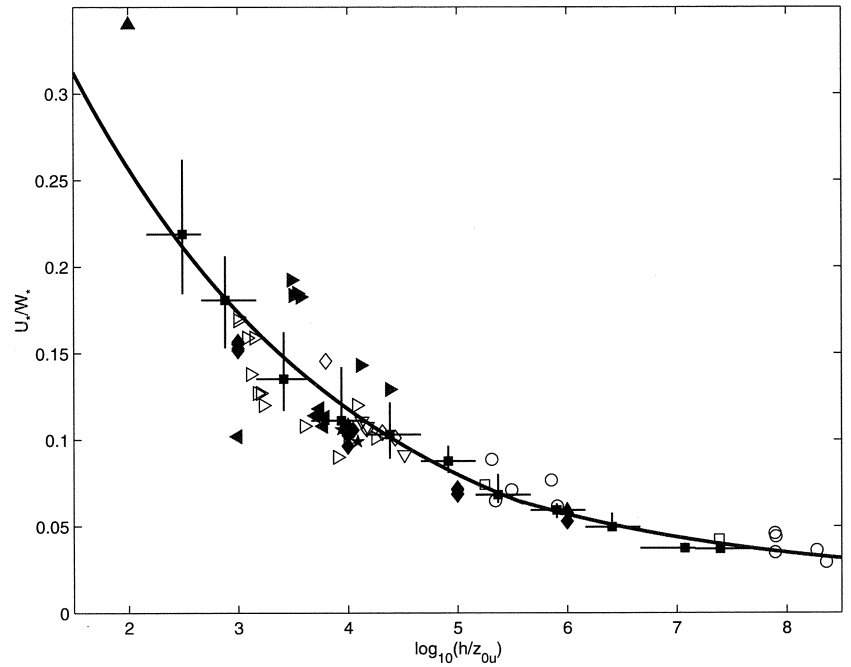

Figure 4. Comparisons of the resistance coefficient U_*/W_* versus roughness h/z_{0u}. The curve shows our LES model: Eq. (41) for the high-roughness surfaces $h/z_{0u} \leqslant 4 \times 10^5$ and Eq. (34) for the low-roughness surfaces, $h/z_{0u} \geqslant 4 \times 10^5$, with empirical coefficients given in Table 4. Open symbols show field data from various field experiments: squares—SCOPE, circles—TOGA COARE over the sea, top-down triangles—BOREX over flat and comparatively smooth land surface, diamond shapes—PAFEX-1, and top-right triangles—ATHENS/ATTIKI over very rough urban canopies. Closed symbols show LES data: squares with error bars—LESNIC database, vertex-up triangles—Schmidt and Schumann (1989), diamonds—Sykes *et al.* (1993), vertex-right triangles—Sorbjan (1996), vertex-left triangles—Otte and Wyngaard (2001), stars—Noh *et al.* (2003). See Table 2 and text for further details.

$L_x \approx L_y \approx 3L_z \approx 4.5h$. The larger horizontal dimensions allow hosting from four (as in Fig. 2) to eight fully developed convective plumes. Figure 3 shows instant structures of resolved temperature fluctuations in LES over very smooth (run 2) and very rough (run 30) surfaces. The fluctuations are averaged over two layers: the surface layer, 150–300 m; and the CBL top, 1650–1800 m.

In all runs, the mean horizontal pressure gradient is set to zero. The surface roughness length for momentum, z_{0u}, and the temperature flux at the surface are prescribed and held constant during the run time. The friction velocity, u_*, is calculated using the log-law at each point of the lowest computational level at every time step. The use of the MO relationships instead of the log-law is shown to be a worse choice, as the algorithm often does not converge. Appendix 1 gives more information about the effect of the boundary conditions on the CBL height, h, and the area-averaged friction velocity, $U_* = \langle |\mathbf{u}'w'| \rangle^{1/2}$.

To achieve statistically stable results, all LES runs are performed over 12 model hours starting from motionless, stratified initial conditions, perturbed by small temperature fluctuations with random amplitude of 0.1 K imposed at the lowest five levels. Then, in order to generate data for the verification of the proposed theory, we average instant values of U_*, h and $\Delta\theta$ (sampled every 10 minutes) over every 30-minute interval from the third through the 12th hour of the simulation. To determine $\Delta\theta = \theta_0 - \theta_a$, we approximate the instant profile of $\langle \theta(z) \rangle$ between the second and the fifth computational

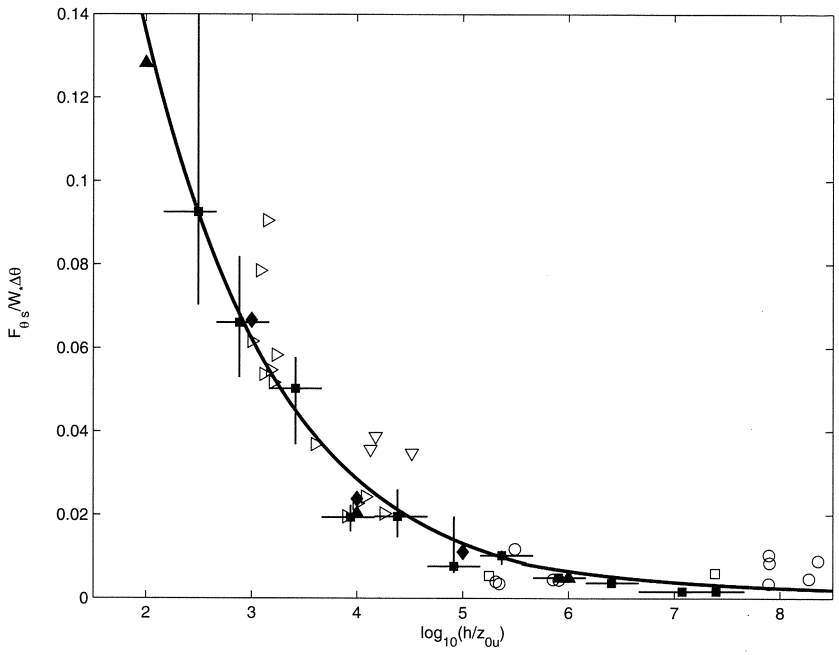

Figure 5. As Fig. 4, but comparisons of the heat-transfer coefficient $F_{\theta s}/(W_*\Delta\theta)$ versus roughness h/z_{0u}. The curve shows Eq. (42) for the high-roughness surfaces $h/z_{0u} \leqslant 4 \times 10^5$, and Eq. (35) for the low-roughness surfaces, $h/z_{0u} \geqslant 4 \times 10^5$; empirical coefficients are given in Table 3.

levels by the 1/3 power-law, and extrapolate it analytically down to the level $z = z_{0u}$ to obtain the aerodynamic surface temperature θ_0. The atmospheric mean potential temperature, θ_a, is calculated directly as the mean value of θ in the CBL core; 900 samples of U_*, $\Delta\theta$ and h obtained by these means exhibited rather large scatter. In Figs. 4 and 5, the data are further averaged within 0.5 $\log(h/z_{0u})$ bins. The error-bars show one standard deviation of the raw data. Good agreement between the LES and the atmospheric data in these figures confirms the robustness of our LES.

(iii) *Earlier LES data.* Shear-free convection has been investigated in numerous LES studies. However, the majority of published papers do not provide complete sets of parameters needed in the present paper (first of all U_* and $\Delta\theta$). Only a few earlier papers were suitable for our purposes. Schmidt and Schumann (1989) performed three LES runs at $h/z_{0u} = 10^2$; 10^4; 10^6, with vertical resolutions of 48 levels. Sykes and Henn (1989) and Sykes *et al.* (1993) performed 14 LES runs clustered around three distinct values of $h/z_{0u} = 10^3$; 10^4; 10^5, with vertical resolutions from 31 to 61 levels. Sorbjan (1996) performed six LES runs in the interval $3 \times 10^3 h/z_{0u} < 2.5 \times 10^4$ with vertical resolutions from 55 to 100 levels; in his LES the free-flow Brunt–Väisälä frequency, N, varied from 0.018 to 1.826 s^{-1}. Otte and Wyngaard (2001) performed five suitable LES runs for h/z_{0u} close to 5×10^3. Noh *et al.* (2003) performed two LES runs for $h/z_{0u} = 8.7 \times 10^3$ and 1.2×10^4 with resolution 80^3. Thus, prior LES studies correspond to values of h/z_{0u} clustered in a few groups, which do not provide enough information to validate our theoretical results, Eqs. (34)–(35) and (41)–(42), over the entire meteorologically meaningful interval $10^2 < h/z_{0u} < 10^9$.

(c) *Validation of model and determination of dimensionless constants*

The proposed model implies that essential features of large-scale eddies, and therefore the heat and mass-transfer in the shear-free convective surface layer, depend on the CBL depth and the surface roughness. Numerous data from field measurements and LES collected in the present paper strongly support this conclusion.

Figure 3 is based on our LES runs 2 and 30; it shows the difference between typical large eddies over smooth and rough surfaces. Bright areas, where the temperature fluctuations $\theta(x, y, z) - \langle\theta\rangle$ are positive, represent updraughts. In the lower part of the CBL over the smooth surface the fluctuations are very well organized into large cells (Fig. 3(a)), whereas over the rough surface the cells look more chaotic (Fig. 3(b)). This difference is even more pronounced in the upper part of the CBL (Figs. 3(c) and (d)).

Similar features of convective structures were observed in the laboratory experiments of Du and Tong (2000). They demonstrated predominantly narrow updraughts separated by wide areas of slow motions over smooth surfaces, in contrast to more densely distributed updraughts separated by equally wide areas of downdraughts with rather intense motions over a very rough surface (their Fig. 6). Comparing these two extreme roughness cases, Du and Tong found that the convective heat transfer was 76% more efficient over the rough surface.

Figures 4 and 5 show theoretical curves representing the resistance law, Eqs. (34) and (41), and the heat-transfer law, Eqs. (35) and (42), together with data from field measurements and LES identified in Table 2. It is worth emphasizing that data from the field experiments and the LES data shown in the figures correlate very well, demonstrating that the LES does indeed realistically reproduce the CBL turbulence. The field data and the LES data both support the proposed theory. Very good correspondence between the LES for $z_{0u} = 1$, 2, 3 and 5 m and observational data over the city of Athens suggests that the hills typical of the Athens area (much lower than the CBL depth) affect the convective air flow in the same way as the roughness elements, and simply increase the effective roughness lengths.

For the very rough surfaces ($h/z_{0u} < 4 \times 10^5$) our Eqs. (41)–(42) predict sharp increases of the resistance and heat-transfer coefficients with decreasing h/z_{0u}, in excellent correspondence with all data. Moreover, the spread of data on the most practically important heat-transfer coefficient is minimal for the roughest surfaces. Fitting the theoretical curves to experimental and LES data gives quite certain estimates of the dimensionless constants: $C_{U3} = 0.54$, $C_{00} = 0.3$ and $C_3 = 0.6$.

For the low-roughness and smooth surfaces ($h/z_{0u} > 4 \times 10^5$) we have fewer data. In particular, we avoided performing LESs of CBLs over aerodynamically smooth surfaces. In this case the effective roughness length no longer depends on the properties of roughness elements but becomes proportional to the depth of the viscous sub-layer: $z_{0u} \sim 10^{-1}\nu/U_*$, where $\nu \sim 1.2 \times 10^{-5}$ m^{2}s^{-1} is the kinematical viscosity of the air. This makes LES modelling of the resistance and heat transfer hardly reasonable, because LES does not include the effects of molecular viscosity and conductivity.

Available data on the resistance coefficient, U_*/W_*, over the interval $4 \times 10^5 < h/z_{0u} < 3 \times 10^8$ confirm our Eq. (34) nearly perfectly, which allows estimation of the dimensionless constants: $C_{U0} = 6$, $C_{U1} = 0.29$ and $C_{U2} = -2.56$. It follows that the aerodynamically rough surface formulation for the momentum transfer holds true up to $h/z_{0u} = 10^8$, that is up to $z_{0u} \sim 10^{-5}$ m (taking the typical value of $h \sim 10^3$ m). Figure 4 gives the minimum value of $U_*/W_* \sim 0.04$. Then, taking $W_* \sim 2$–3 m s^{-1}, yields $U_* \sim 10^{-1}$ m s^{-1} and therefore the maximal value of smooth-surface roughness

TABLE 2. SUMMARY OF LES AND FIELD DATA, AND CORRESPONDING SYMBOLS IN FIGS. 4 AND 5

LES data	Closed symbols	Reference
Present LES	Squares with vertical and horizontal bars	Vertical error bars denote one standard deviation of the 30-minute samples averaged within a bin; horizontal bars show the bin width. The samples are taken every 10 minutes between the third and 12th hours of the CBL growth, averaged horizontally at every instant and then additionally averaged over 30-minute time intervals
Schmidt and Schumann LES	Vertex-up triangles	Schmidt and Schumann (1989)
Sykes *et al.* LES	Diamonds	Sykes *et al.* (1993)
Sorbjan LES	Vertex-right triangles	Sorbjan (1996)
Otte and Wyngaard LES	Vertex-left triangles	Otte and Wyngaard (2001)
Noh *et al.* LES	Stars	Noh *et al.* (2003)

Field data	Open symbols	Reference
SCOPE, September 1993, San Clemente Island, California	Squares	
TOGA COARE, 1992–1993, Western Pacific Ocean	Circles	Fairall *et al.* (1996a,b,c) Grachev and Fairall (1997) Grachev *et al.* (1997, 1998)
BOREX, July 1995, Borris site, Denmark	Vertex-down triangles	Mikkelsen *et al.* (1996) Grachev *et al.* (1998)
PAFEX-1, January–February 1998, Phoenix, Arizona	Diamonds	Grachev *et al.* (1999)
ATHENS, 1994–99, Athens city centre and Attiki peninsula, Greece	Vertex-right triangles	Batcharova and Gryning (1998) Akylas *et al.* (2003)

See text for acronyms.

length: $z_{0u} \sim 10^{-1}\nu/U_* \sim 10^{-5}$ m. Thus Eq. (34) with the above empirical constants is definitely applicable up to $h/z_{0u} < 10^8$. At larger h/z_{0u}, it is reasonable to expect a transition to the aerodynamically smooth surface regime with the resistance coefficient practically independent on the size and shape of roughness elements and presumably constant: $U_*/W_* = 4 \times 10^{-2}$.

Experimental data on the heat-transfer coefficient, $F_{\theta s}/(W_*\Delta\theta)$, shown in Fig. 5 confirm our Eq. (35) in the interval $4 \times 10^5 < h/z_{0u} < 5 \times 10^7$, and give the following estimates of the dimensionless constants: $C_1 = 0.17$, $C_2 = -2.5$. But at $h/z_{0u} \sim 10^8$ the data (from TOGA COARE) become rather uncertain, and show an increase of $F_{\theta s}/(W_*\Delta\theta)$ with increasing h/z_{0u}, which does not look physically grounded; it could be caused by low accuracy in the determination of the roughness length of the sea surface in calm weather convection. To clarify this issue, further high-quality experiments are needed.

The recommended resistance and heat-transfer formulations, the empirical constants in these formulations, and the matching point between the high-roughness, the low-roughness and the aerodynamically smooth surface regimes, are summarized in Table 3.

5. CONCLUSIONS

As in prior models of Businger (1973a,b), Schumann (1988), Sykes *et al.* (1989) and Zilitinkevich *et al.* (1988) and the more practically oriented papers of Beljaars

(1994) and Redelsperger *et al.* (2000), it is demonstrated that the Prandtl, Obukhov, and MO similarity theories of the atmospheric surface-layer turbulence, as well as other local theories and turbulence closures, become inadequate in shear-free convection. In this regime, basic features of the surface layer are strongly affected by large-scale semi-organized convective eddies characterized by the length-scale h (CBL depth) and the velocity-scale $W_* = (F_{bs}h)^{1/3}$, both overlooked in the classical theories of the surface layer.

Although the key non-local mechanism for enhancing the turbulence, namely, strong shears in the near-surface convergence flow patterns driven by large eddies, has already been recognized, none of the prior models is applicable to the entire meteorological range of roughness lengths and CBL depths.

The model proposed here accounts for the dependence of the effective roughness length on the buoyancy flux (besides its well-known dependence on the surface-roughness geometry), and covers the whole range of convection regimes over natural surfaces varying from extremely rough to aerodynamically smooth ($10^2 < h/z_{0u} < 10^8$). It is more consistent with experimental and LES data than previous models, which showed good correspondence with data only within limited intervals of h/z_{0u}.

The basic result from this work is the new heat-transfer law (Eqs. (35) and (42)) comprehensively verified against experimental and LES data. It predicts a sharp decrease of the coefficient $F_{\theta s}/(W_*\Delta\theta)$ with increasing h/z_{0u}, in excellent correspondence with experimental and LES data (see Fig. 5).

By contrast, the classical heat-transfer law (Eqs. (10) and (11)) does not imply any dependence on the roughness length, z_{0u}. Instead, it employs the depth of the molecular conductivity sub-layer, $\delta_\kappa = \kappa/W_*$, and can be rewritten as:

$$\frac{F_{\theta s}}{W_*\Delta\theta} = \frac{C_{\mathrm{conv}}^{3/4}}{\mathrm{Pr}^{1/4}}\left(\frac{h}{\delta_\kappa}\right)^{-1/4}. \tag{43}$$

To demonstrate the difference, we compare in Fig. 6 the alternative theoretical estimates of $F_{\theta s}/(W_*\Delta\theta)$ for the typical atmospheric CBL, with $h = 10^3$ m and $W_* = 1$ m s^{-1}, over a range of surfaces from very rough ($z_{0u} = 1$ m) to unrealistically smooth (with z_{0u} defined as 1/25 of the typical height of roughness elements $= 10^{-7}$ m). In this format Eq. (43), which does not include z_{0u}, is shown in Fig. 6 by the dashed line parallel to the abscissa: $F_{\theta s}/(W_*\Delta\theta) = 0.0025$ (calculated taking $\kappa = 10^{-5}$ m^{2}s^{-1}, $\mathrm{Pr} = \nu/\kappa = 1$ and $C_{\mathrm{conv}} = 0.14$); our Eqs. (35) and (42) are shown by the solid line (equivalent to the solid line in Fig. 5).

Recall that the minimum possible value of the effective roughness length, achieved over aerodynamically smooth surfaces, is $z_{0u} = 0.1\nu/U_*$, that is in our case $z_{0u} = 3 \times 10^{-5}$ m (taking $\nu = 10^{-5}$ m^{2}s^{-1} and the minimum value of $U_* = 0.04$ m s^{-1} from the dataset represented in Fig. 4).

As seen from Fig. 6, the classical heat-transfer law (known to be a reasonable approximation in laboratory experiments) is absolutely inapplicable to nearly the entire interval of roughness lengths typical of the land and the sea surfaces, $1\ \mathrm{m} < z_{0u} < 3 \times 10^{-5}$ m.

In future work the horizontal and vertical profiles and other features of our model deserve further investigation using conditional sampling of measurements or LES in the internal boundary layer in relation to the locations of the plumes (e.g. as in Hunt *et al.* 2003). The increasing roughness length associated with small-scale thermal plumes rising between the roughness elements also needs to be studied in detail.

TABLE 3. RECOMMENDED FORMULAE AND DIMENSIONLESS CONSTANTS

Constant	Value of constant	Formula	Interval of applicability
C_{U3} C_{00}	0.54 0.3	$\dfrac{U_*}{W_*} = C_{U3}\left\{\dfrac{z_{0u}}{h} + C_{00}\left(\dfrac{z_{0u}}{h}\right)^{8/7}\right\}^{1/6}$ Eq. (41)	$\dfrac{h}{z_{0u}} < 4 \times 10^5$
C_{U0} C_{U1} C_{U2}	6 0.29 −2.56	$\dfrac{U_*}{W_*} = C_{U1}\left(\ln\dfrac{h/z_{0u}}{(\ln(h/z_{0u}) - C_{U0})^3} + C_{U2}\right)^{-1}$ Eq. (34)	$4 \times 10^5 < \dfrac{h}{z_{0u}} < 10^8$
		$\dfrac{U_*}{W_*} = 3 \times 10^{-2}$	$\dfrac{h}{z_{0u}} > 10^8$
C_3	0.6	$\dfrac{F_{\theta s}}{W_*\Delta\theta} = \dfrac{F_{qs}}{W_*\Delta q} = \dfrac{W_*^2}{(\beta\Delta\theta + 0.61g\Delta q)h} = C_3\left\{\dfrac{z_{0u}}{h} + C_{00}\left(\dfrac{z_{0u}}{h}\right)^{8/7}\right\}^{1/3}$ Eq. (42)	$\dfrac{h}{z_{0u}} < 4 \times 10^5$
C_1 C_2	0.17 −2.5	$\dfrac{F_{\theta s}}{W_*\Delta\theta} = \dfrac{F_{qs}}{W_*\Delta q} = \dfrac{W_*^2}{(\beta\Delta\theta + 0.61g\Delta q)h}$ $= C_1\left(\ln\dfrac{h/z_{0u}}{(\ln(h/z_{0u}) - C_{U0})^3} + C_{U2}\right)^{-1}\left(\ln\dfrac{h/z_{0u}}{(\ln(h/z_{0u}) - C_{U0})^3} + C_2\right)^{-1}$ Eq. (35)	$4 \times 10^5 < \dfrac{h}{z_{0u}} < 10^8$

See text for details.

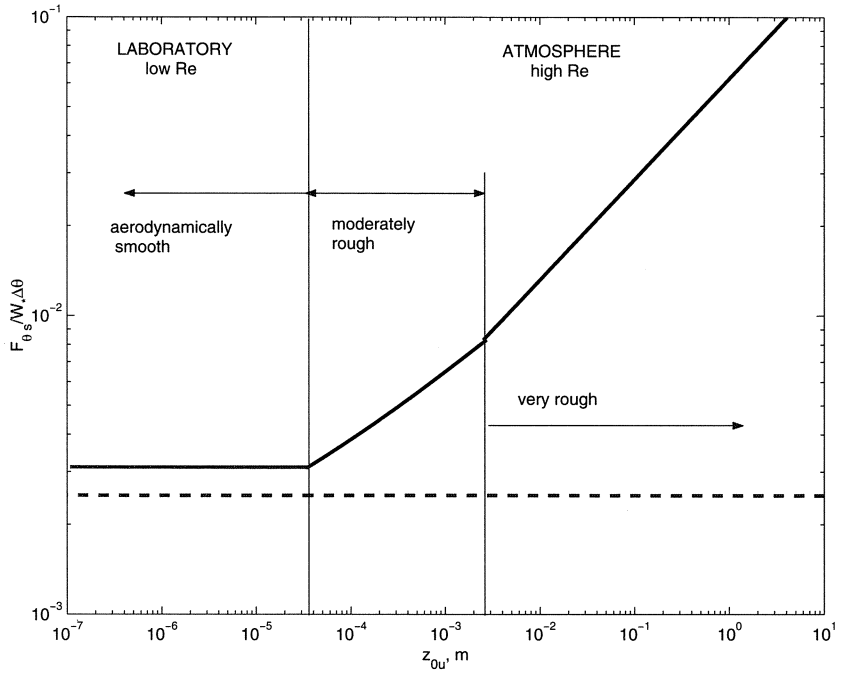

Figure 6. Comparison of two alternative heat-transfer models for the shear-free convective boundary layer (CBL). The solid line shows Eqs. (35) and (42) validated through atmospheric measurements and large-eddy simulation. The minimum effective roughness length in our model is $z_{0u} = 0.1\nu/U_* = 3.6 \times 10^{-5}$ m. The dashed line shows the traditional formulation given by Eqs. (10), (11) or (43) validated through lab experiments. In atmospheric CBLs over typical natural surfaces, it underestimates the heat transfer by up to two orders of magnitude. See text for details.

To proceed towards improved parametrization of the surface fluxes in large-scale models, the proposed theory should be extended in order to account for the mean wind shear. Relying on Fig. 4, it is conceivable that the enhancing effect of large convective eddies must be pronounced, and should be taken into account until the friction velocity caused by the mean wind shear becomes at least an order of magnitude larger than the Deardorff velocity-scale, W_*.

ACKNOWLEDGEMENTS

This work has been supported by the EU Marie Curie Chair Project MEXC-CT-2003-509742, EU Project FUMAPEX EVK4-2001-00281, Norwegian project MACESIZ 155945/700, joint Norwegian-USA project ROLARC 151456/720, and the NORDPLUS Neighbour 2005-2006 Project FI-51. JCRH and SSZ were supported by NERC at CPOM at UCL. JCRH, AAG, HJSF acknowledge support from NSF for the PAFEX project in 1998.

APPENDIX

Quality assessment of our LES

The quality of CBL simulations using LES codes is regularly discussed in the literature. A straightforward way to assess it is to gradually refine the model resolution, and to check whether relevant physical parameters obtained through a LES are not

TABLE A.1. EXTERNAL AND INTERNAL (CALCULATED) PARAMETERS OF LES RUN 31 AND ITS MODIFICATIONS

Run	Numerical resolution $N_x \times N_y \times N_z$	Domain size (km) $Lx \times Ly \times Lz$	U_* (m s^{-1})	W_* (m s^{-1})	$\Delta\theta$ (K)	h (m)	Σ_U (%)	Σ_θ (%)
31	64 × 64 × 64	3.6 × 3.6 × 1.2	0.11	1.11	0.3	413	0	0
31a	128 × 128 × 128	3.6 × 3.6 × 1.2	0.14	1.11	0.4	413	26	26
31b[1]	64 × 64 × 64	3.6 × 3.6 × 1.2	0.13	1.13	0.4	431	16	26

[1]Run 31b used non-slip surface boundary conditions. See text for details.

significantly changed. Khanna and Brasseur (1997) employed high-resolution LESs (with the finest vertical resolution ~4.2 m) to demonstrate that the turbulence statistics in the surface layer are much more sensitive to the subgrid closure than to the model resolution. Agee and Gluhovsky (1999) analysed several independent LESs of CBLs with different resolution and found quite low sensitivity of the low order statistics to the LES resolution, provided that the vertical resolution was finer than ~50 m. Chandrasekar *et al.* (2003) found a good correspondence between LES and data from the summer NE-OPS campaign, using a stretched mesh with vertical resolution as coarse as 100 m in the CBL core. Our experience confirms these conclusions.

Successful representation of CBLs through coarse-resolution LESs calls for a physical explanation. Meyers and Baelmans (2004) estimated theoretically the LES resolution required to reproduce isotropic turbulence at a certain level of accuracy. According to their analyses, 48^3 grid nodes in a volume h^3 are sufficient to explicitly resolve 95% of the turbulent kinetic energy. It follows that large convective eddies in the CBL core can indeed be resolved reasonably accurately even in a coarse LES. Hunt and Morrison (2000) argued that integral properties of the surface-layer turbulence strongly depend on descending coherent eddies. Högstroem *et al.* (2002) and Hong *et al.* (2004) supported this argument using data from atmospheric measurements. Proceeding to LESs, it is conceivable that realistic simulation of large (and therefore well-resolved) coherent eddies in the CBL core causes quite correct representation of integral properties of small under-resolved eddies in the surface layer. Mayor *et al.* (2003) corroborated this idea; they demonstrated surprisingly good statistical and even structural qualities of the coarse LES compared with lidar data in the surface layer where, at first sight, the model should be expected to perform poorly.

The above short literature survey suggests that our LES runs, with 30–50 levels within the CBL, should reproduce basic properties of the shear-free CBL reasonably accurately. Additionally, to evaluate the quality of our LES we have carried out several sensitivity simulations. LES run 31 (see Tables 1 and A.1) was used as the basic simulation; we repeated it with twice the resolution (128^3, run 31a), and with the standard resolution (64^3) but using non-slip surface boundary conditions (run 31b). Other parameters of the new runs were kept the same as in the original run 31. The output parameters from all three runs are given in Table A.1, in which the last two columns present deviations, Σ_U and Σ_θ, of the resistance coefficient, U_*/W_*, and the heat-transfer coefficient, $F_{\theta s}/(W_*\Delta\theta)$, respectively, from those in run 31:

$$\Sigma_R \frac{|U_*^{xx}/W_*^{xx} - U_*^{31}/W_*^{31}|}{U_*^{31}/W_*^{31}} * 100,$$
$$\Sigma_\theta = \frac{|F_{\theta s}^{xx}/(W_*^{xx}\Delta\theta^{xx}) - F_{\theta s}^{31}/(W_*^{31}\Delta\theta^{31})|}{F_{\theta s}^{31}/(W_*^{31}\Delta\theta^{31})} * 100, \tag{A.1}$$

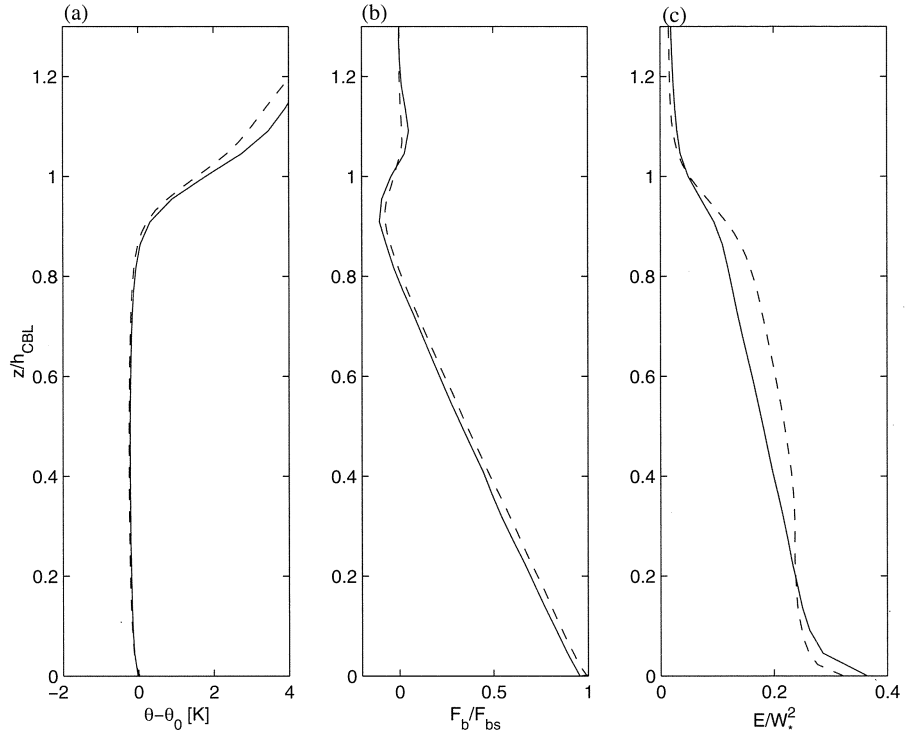

Figure A.1. Comparison of the convective boundary layer (CBL) vertical profiles in our large-eddy simulation model of the basic calculated parameters averaged in the horizontal (over the domain cross-sections) and over time (1 h), in run 31 (resolution 64^3, $\Delta_z = 18.75$ m, solid curves), and in the fine-resolution run 31a (resolution 128^3, $\Delta_z = 9.38$ m, dashed curves): (a) the air–surface temperature difference; (b) the buoyancy flux normalized by its surface value; (c) the turbulent kinetic energy normalized by Deardorff's velocity-scale. The height is normalized by the CBL depth defined as the height of the maximum temperature gradient.

where superscripts 31 and xx indicate run 31 and the compared run, respectively. It follows that the uncertainty caused by the choice of the surface boundary conditions, numerical resolution and limitations on the computational domain, is about 25%.

Figure A.1 shows the differences between runs 31 and 31a. Clearly, only the turbulent kinetic energy profiles in these runs (Fig. A.1(c)) differ significantly. Better representation of the thin surface-shear layer in run 31a results in larger values of the fluctuation velocity and the surface–air temperature difference. However, the difference between runs 31 and 31a is less than the typical scatter in LES runs. Run 31a has the finest physical and numerical resolution among the LES runs available from literature.

REFERENCES

Agee, E. and Gluhovsky, A. 1999 LES model sensitivities to domain, grids, and large-eddy timescales. *J. Atmos. Sci.*, **56,** 599–604

Akylas, E., Tombrou, M., Lalas, D. and Zilitinkevich, S. 2001 Surface fluxes under shear-free convection. *Q. J. R. Meteorol. Soc.*, **127,** 1–15

Akylas, E., Tsakos, Y., Tombrou, M. and Lalas, D. P. 2003 Consideration on minimum friction velocity. *Q. J. R. Meteorol. Soc.*, **129**(591), 1929–1943

Armfield, S. and Street, R. 1999 The fractional step method for the Navier–Stokes equations on staggered grids: The accuracy of three variations. *J. Comput. Phys.*, **153,** 660–665

Baklanov, A., Mestayer, P., Clappier, A., Zilitinkevich, S., Joffre, S., Mahura, A. and Nielsen, N. W. 2005 On parameterizations of the urban atmosphere sublayer in meteorological models. *Atmos. Chem. Phys. Discuss.*, **5,** 12119–12176

Batcharova, E. and Gryning, S. E. 1998 Meteorological measurements, wind climatology, atmospheric turbulence and internal boundary layer development in Athens during the Medcaphot-Trace Experiment. *Atmos. Environ.*, **32,** 2055–2069

Beare, R. J., MacVean, M. K., Holtslag, A. A. M., Cuxart, J., Esau, I., Golaz, J.-C., Jimenez, M. A., Khairoutdinov, M., Kosovic, B., Lewellen, D., Lund, T. S., Lundquist, J. K., McCabe, A., Moene, A. F., Noh, Y., Raasch S. and Sullivan, P. 2006 An intercomparison of large-eddy simulations of the stable boundary layer. *Boundary Layer Meteorol.* In press

Belcher, S. E., Jerram, N. and Hunt, J. C. R. 2003 Adjustment of a turbulent boundary layer to a canopy of roughness elements. *J. Fluid Mech.*, **448,** 369–398

Beljaars, A. C. M. 1994 The parameterization of surface fluxes in large-scale models under free convection. *Q. J. R. Meteorol. Soc.*, **121,** 255–270

Beljaars, A. C. M. and Holtslag, A. A. M. 1991 Flux parameterization over land surfaces for atmospheric models. *J. Appl. Meteorol.* **30,** 327–341

Berkooz, G., Holmes, P. and Lumley, J. L. 1993 The proper orthogonal decomposition in the analysis of turbulent flows. *Ann. Rev. Fluid Mech.*, **25,** 539–575

Businger, J. A. 1973a A note on free convection. *Boundary-Layer Meteorol.* **4,** 323–326

1973b Turbulent transfer in the atmospheric surface layer. Pp. 67–100 in *Workshop in micrometeorology*. Ed. D. A. Haugen. American Meteorological Society, Boston, USA

Canuto, V. M. and Minotti, F. 1993 Stratified turbulence in the atmosphere and oceans: A new subgrid model. *J. Atmos. Sci.*, **50,** 1925–1935

Chandrasekar, A., Philbrick, C. R., Clarc, R., Doddridged, B. and Georgopoulos, P. 2003 A large-eddy simulation study of the convective boundary layer over Philadelphia during the 1999 Summer NE-OPS campaign. *J. Env. Fluid Mech.*, **3,** 305–329

Coelho, S. L. V. and Hunt. J. C. R. 1989 Vorticity dynamics of the near field of strong jets in cross flows. *J. Fluid Mech.*, **200,** 411–445

Deardorff, J. W. 1970 Convective velocity and temperature-scales for the unstable planetary boundary layer. *J. Atmos. Sci.*, **27,** 1211–1213

1972a Numerical investigation of neutral and unstable planetary boundary layers. *J. Appl. Meteorol.*, **11,** 91–115

1972b Parameterization of planetary boundary layer for use in general circulation models. *Mon. Weather Rev.*, **2,** 93–106

Deardorff, J. W., Willis, G. E. and Stockton, B. H. 1980 Laboratory studies of the entrainment zone of a convectively mixed layer. *J. Fluid Mech.*, **100,** 41–64

Du, Y.-B. and Tong, P. 2000 Turbulent thermal convection in a cell with ordered rough boundaries. *J. Fluid Mech.*, **407,** 57–84

Elperin, T., Kleeorin, N., Rogachevskii, I. and Zilitinkevich, S. 2002 Formation of large-scale semi-organised structures in turbulent convection. *Phys. Rev. E.*, **66,** 066305, 1–15

2006 Turbulence and coherent structures in geophysical convection. *Boundary-layer Meteorol.* In press

Esau, I. 2003 The Coriolis effect on coherent structures in planetary boundary layers. *J. Turbulence*, **4,** 017

Esau, I. N. 2004 Simulation of Ekman boundary layers by a large eddy model with dynamic mixed subfilter closure. *Env. Fluid Mech.*, **4**(3), 273–303

Fairall, C. W., Bradley, E. F., Rogers, D. P., Edson, J. B. and Young, G. S. 1996a Bulk parameterization of air–sea fluxes for the Tropical Ocean-Global Atmosphere Coupled-Ocean Atmosphere Response Experiment. *J. Geophys. Res.*, **101**(C2), 3747–3764

Fairall, C. W., Godfrey, J. S., Wick, G. A., Edson, J. B. and Young, G. S. 1996b Cool-skin and warm layer effects on sea surface temperature. *J. Geophys. Res.*, **101**(C1), 1295–1308

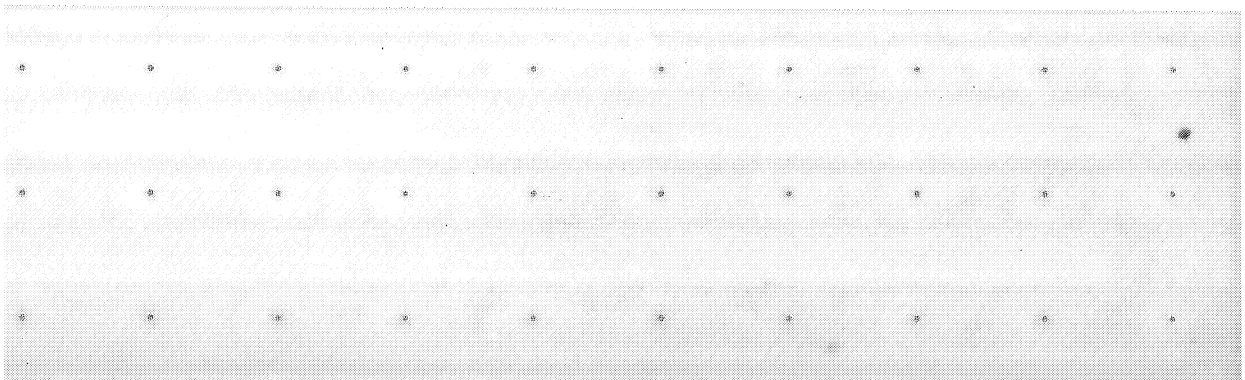

Fairall, C. W., Grachev, A. A., Bedard, A. J. and Nishiyama, R. T. 1996c 'Wind, wave, stress, and surface roughness relationships from turbulence measurements made on R/P FLIP in the SCOPE Experiment'. NOAA Technical Memorandum, ERL ETL 268, Boulder, Colorado, USA, April 1996 (available from the National Technical Information Service, 5285 Port Royal Rd., Springfield, VA 22161)

Fairall, C. W., White, A. B., Edson, J. B. and Hare, J. E. 1997 Integrated shipboard measurements of the marine boundary layer. *J. Atmos. Oceanic Technol.*, **14,** 338–359

Fedorovich, E., Conzemius, R., Esau, I., Chow, F., Lewellen, D., Moeng, C.-H., Sullivan, P., Pino, D. and Vila-Guerau de Arellano, J. 2004 'Entrainment into sheared convective boundary layers as predicted by different large eddy simulation codes'. In Proceedings of the 16th AMS conference on boundary layers and turbulence. American Meteorological Society, Boston, USA

Golitsyn, G. S. 1979 Simple theoretical and experimental study of convection with some geophysical applications and analogies. *J. Fluid Mech.* **95,** 567–608

Golitsyn, G. S. and Grachev, A. A. 1986 Free convection of multi-component media and parameterization of air–sea interaction at light winds. *Ocean–Air Interactions*, **1,** 57–78

Grachev, A. A. 1989 Temperature profile and heat transfer in free turbulent convection near a horizontal surface. *Izvestiya, Acad. Sci., USSR, Atmos. Oceanic Phys.* **25**(2), 837–846 (English Edition)

Grachev, A. A. and Fairall, C. W. 1997 Dependence of the Monin–Obukhov stability parameter on the bulk Richardson number over the ocean. *J. Appl. Meteorol.*, **36**(4), 406–414

Grachev, A. A., Fairall, C. W. and Zilitinkevich, S. S. 1997 Surface-layer scaling for the convection-induced stress regime. *Boundary-Layer Meteorol.*, **83,** 423–439

Grachev, A. A., Fairall, C. W. and Larsen, S. E. 1998 On the determination of the neutral drag coefficient in the convective boundary layer. *Boundary-Layer Meteorol.*, **86**(2), 257–278

Grachev, A. A., Fernando, H. J. S., Hunt, J. C. R., Pardyjak, E. P., Oroud, I., Berman, N., Yu, F. and Wang, G. 1999 'The structure of the atmospheric boundary layer over the complex terrain of Phoenix Valley'. Pp. 331–334 in Preprints of the 79th AMS Annual Meeting, 13th Symposium on boundary layers and turbulence, Dallas TX, 10–15 January 1999. American Meteorological Society, Boston, USA

Hibberd, M. F. and Sawford, B. L. 1994 A saline laboratory model of the planetary convective boundary layer. *Boundary-Layer Meteorol.* **67,** 229–250

Högström, U., Hunt, J. C. R. and Smedman, A.-S. 2002 Theory and measurements for turbulence spectra and variances in the atmospheric neutral surface layer. *Boundary-Layer Meteorol.*, **103,** 101–124

Hong, J., Choi, T., Ishikawa, H. and Kim, J. 2004 Turbulence structures in the near-neutral surface layer on the Tibetan Plateau. *Geophys. Res. Lett.*, **31,** L15106, doi: 10.1029/2004GL019935

Howard, L. N. 1990 Limits of the transport of heat and momentum by turbulent convection with large-scale flow. *Stud. Appl. Math.* **83,** 273–285

Hunt, J. C. R. 1984 Turbulence structure in thermal convection and shear-free boundary layers. *J. Fluid Mech.*, **138,** 161–184

Hunt, J. C. R. and Durbin, P. A. 1999 Perturbed vortical layers and shear sheltering. *Fluid Dyn. Res.*, **24,** 375–404

Hunt, J. C. R. and Morrison, J. F. 2000 Eddy structure in turbulent boundary layers, *Eur. J. Mech. B – Fluids*, **19,** 673–694

Hunt, J. C. R., Kaimal, J. C. and Gaynor, J. I. 1988a Eddy structure in the convective boundary layer—new measurements and new concepts. *Q. J. R. Meteorol. Soc.* **114,** 837–858

Hunt, J. C. R., Leibovich, S. and Richards, K. J. 1988b Turbulent shear flows over low hills. *Q. J. R. Meteorol. Soc.*, **114,** 1435–1470

Hunt, J. C. R., Vrieling, A. J., Nieuwstadt, F. T. M. and Fernando, H. J. S. 2003 The influence of the thermal diffusivity of the lower boundary on eddy motion in convection. *J. Fluid Mech.*, **491,** 183–205

Kader, B. A. and Yaglom, A. M. 1990 Mean fields and fluctuation moments in unstably stratified turbulent boundary layers. *J. Fluid Mech.* **212,** 637–662

Khanna, S. and Brasseur, J. G. 1997 Analysis of Monin–Obukhov similarity from large-eddy simulations. *J. Fluid. Mech.*, **345,** 251–286

Langford, J. and Moser, R. D. 1999 Optimal LES formulations for isotropic turbulence. *J. Fluid Mech.*, **398,** 321–346

Lenschow, D. H., Wyngaard, J. C. and Pennell, W. T. 1980 Mean-field and second-moment budgets in a baroclinic, convective boundary layer. *J. Atmos. Sci.*, **37,** 1313–1326

Liu, S., Meneveau, C. and Katz, J. 1994 On properties of similarity subgrid-scale models as deduced from measurements in a turbulent jet. *J. Fluid Mech.*, **275,** 83–119

Liu, W. T., Katsaros, K. B. and Businger, J. A. 1979 Bulk parameterization of air–sea exchange of heat and water vapour including the molecular constants at the interface. *J. Atmos. Sci.* **36,** 1722–1735

Louis, J. F. 1979 A parametric model of vertical eddy fluxes in the atmosphere. *Boundary-Layer Meteorol.*, **17,** 187–202

Malkus, W. V. R. 1954 The heat transport and spectrum of thermal turbulence. *Proc. R. Soc. London* **A225,** 196–212

Mayor, S. D., Tripoli, G. J. and Eloranta, E. W. 2003 Evaluating large-eddy simulations using volume imaging lidar data. *Mon. Weather Rev.*, **131,** 1428–1452

Meyers, J. and Baelmans, M. 2004 Determination of subfilter energy in large-eddy simulations. *J. Turbulence*, **5,** 026

Mikkelsen, T., Jorgensen, H. E., Lofstrom, P. and Lyck, E. 1996 'Borex-95: Atmospheric dispersion experiment on concentration fluctuations'. Data Report RISØ-R-927(EN). Available from Department of Wind Energy and Atmospheric Physics, Riso National Laboratory, Roskilde, Denmark

Moeng, C.-H. and Wyngaard, J. C. 1989 Evaluation of turbulent transport and dissipation closures in second-order modelling. *J. Atmos. Sci.*, **46,** 2311–2330

Moeng, C.-H., Cotton, W. R., Stevens, B., Bretherton, C., Rand, H. A., Chlond, A., Khairoutdinov, M., Krueger, S., Lewellen, W. S., MacVean, M. K., Pasquier, J. R. M., Siebesma, A. P. and Sykes, R. I. 1996 Simulation of a stratocumulus-topped planetary boundary layer: Intercomparison among different numerical codes. *Bull. Am. Meteorol. Soc.*, **77**(2), 261–278

Moin, P. and Moser, R. D. 1989 Characteristic-eddy decomposition of turbulence in a channel, *J. Fluid. Mech.*, **200,** 471–509

Monin, A. S. and Obukhov, A. M. 1954 Basic laws of turbulence mixing in the surface layer of the atmosphere. *Trudy Geofiz. Inst. AN SSSR*, **24**(151), 163–187

Monin, A. S. and Yaglom, A. M. 1971 *Statistical fluid mechanics*. Vol. 1. MIT Press, Cambridge MA, USA

Morinishi, Y., Lund, T. S., Vasilyev, O. V. and Moin, P. 1998 Fully conservative higher order finite difference schemes for incompressible flow. *J. Comput. Phys.* **143,** 90–124

Nieuwstadt, F. T. M., Mason, P. J., Moeng, C.-H. and Schumann, U. 1993 Large-eddy simulation of the convective boundary layer: A comparison of four computer codes. Pp. 343–367 in *Turbulent shear flows*. Eds. F. Durst, R. Friedrich, B. E. Launder, F. W. Schmidt, U. Schumann and J. H. Whitelaw. Springer, Berlin, Germany

Noh, Y., Cheon, W. G., Hong, S. Y. and Raasch, S. 2003 Improvement of the K-profile model for the planetary boundary layer based on large eddy simulation data. *Boundary-Layer Meteorol.*, **107,** 401–427

Obukhov, A. M. 1946 Turbulence in a thermally heterogeneous atmosphere. *Trudy Inst. Teoret. Geofiz. AN SSSR*, **1,** 95–115

1960 Structure of temperature and velocity fields under conditions of free convection. *Izvestiya AN SSSR, Ser. Geofiz.*, No. 9, 1392–1396

Otte M. J. and Wyngaard, J. C. 2001 Stably stratified interfacial-layer turbulence from large eddy simulation. *J. Atmos. Sci.*, **58,** 3424–3442

Owinoh, A. Z., Hunt, J. C. R., Orr, A., Clark, P., Klein, R., Fernando, H. J. S. and Nieuwstadt, F. T. N. 2005 Effects of changing surface heat flux on the atmospheric boundary layer flow over flat terrain. *Boundary Layer Meteorol.*, **116,** 331–361

Panofsky, H. A., Tennekes, H., Lenschow D. H. and Wyngaard, J. C. 1977 The characteristics of turbulent velocity components in the surface layer under convective conditions. *Boundary-Layer Meteorol.*, **11,** 355–361

Prandtl, L. 1932 Meteorologische Anvendungen der Strömungslehre. *Beitr. Phys. Fr. Atmos.*, **19,** 188–202

Priestley, C. H. B. 1954 Convection from a large horizontal surface. *Austr. J. Phys.*, **7,** 176–202

1959 *Turbulent transfer in the lower atmosphere*. Chicago University Press, Chicago, USA

Rampanelli, D. and Zardi, D. 2004 A method to determine the capping inversion of the convective boundary layer. *J. Appl. Meteorol.*, **43,** 925–933

Rao, K. G. and Narasimha, R. 1996 Estimation of drag coefficient at low wind speeds over the monsoon trough land region during MONTBLEX-90. *Geophys. Res. Lett.*, **23,** 2617–2620

Redelsperger, J. L., Guichard, F. and Mondon, S. 2000 A parameterization of mesoscale enhancement of surface fluxes for large-scale models. *J. Climate*, **13,** 402–421

Schmidt, H. and Schumann, U. 1989 Coherent structure of the convective boundary layer derived from large-eddy simulations. *J. Fluid Mech.* **200,** 511–562

Schumann, U. 1988 Minimum friction velocity and heat transfer in the rough surface layer of a convective boundary layer. *Boundary-Layer Meteorol.*, **44,** 311–326

Siggia, E. D. 1994 High Rayleigh number convection. *Ann. Rev. Fluid Mech.*, **26,** 137–168

Smagorinsky, J. W. 1993 Some historical remarks on the use of nonlinear viscosities. Pp. 3–36 in *Large eddy simulation of complex engineering and geophysical flows*. Eds. B. Galperin and S. A. Orszag. Cambridge University Press, New York, USA

Sorbjan, Z. 1996 Effects caused by varying the strength of the capping inversion based on a large eddy simulation model of the shear-free convective boundary layer. *J. Atmos. Sci.*, **53,** 2015–2024

Stevens, D. E. and Bretherton, C. S. 1999 Effects of grid resolution on large-eddy simulation of radiatively driven entrainment through a strong inversion. *Q. J. R. Meteorol. Soc.*, **125,** 425–439

Sullivan, P. P., McWilliams, J. C. and Moeng, C.-H. 1994 A subgrid-scale model for large-eddy simulation of planetary boundary-layer flows, *Boundary-Layer Meteorol.*, **71,** 247–276

Sullivan, P. P., Horst, T. W., Lenschow, D. H., Moeng, C.-H. and Weil, J. C. 2003 Structure of subfilter-scale fluxes in the atmospheric surface layer with application to large-eddy simulation modelling. *J. Fluid Mech.*, **482,** 101–139, doi: 10.1017/S0022112003004099

Sykes, R. I. and Henn, D. S. 1989 Large-eddy simulation of turbulent sheared convection. *J. Atmos. Sci.*, **46,** 1106–1118

Sykes, R. I., Henn, D. S. and Lewellen, W. S. 1993 Surface-layer description under free-convection conditions. *Q. J. R. Meteorol. Soc.* **119,** 409–421

Turner, J. S. 1973 *Buoyancy effects in fluids*. Cambridge University Press, Cambridge, UK

Vreman, B., Geurts, B. and Kuerten, H. 1994 On the formulation of the dynamic mixed subgrid-scale model. *Phys. Fluids*, **6,** 4057–4059

Webster, P. J. and Lukas, R. 1990 TOGA COARE: The coupled ocean–atmosphere response experiment. *Bull. Am. Meteorol. Soc.*, **73,** 1377–1416

Williams, A. G. and Hacker, J. M. 1992 The composite shape and structure of coherent eddies in the convective boundary layer. *Boundary-Layer Meteorol.*, **61,** 213–245

1993 Interaction between coherent eddies in the lower convective boundary layer, *Boundary-Layer Meteorol.*, **64,** 55–74

Williams, A. G., Kraus, H. and Hacker, J. M. 1996 Transport processes in the tropical warm pool boundary layer. I: Spectral composition of fluxes, *J. Atmos. Sci.*, **53,** 1187–1202

Wilson, D. 1996 Empirical orthogonal function analysis of weakly convective atmospheric boundary layer. I: Eddy structure. *J. Atmos. Sci.*, **53,** 801–823

Wyngaard, J. C. and Cote, O. R. 1974 The evolution of a convective planetary boundary layer—a higher-order-closure model study. *Boundary-Layer Meteorol.*, **7,** 289–308

Yaglom, A. M. 1994 Fluctuation spectra and variances in convective turbulent boundary layers: A re-evaluation of old models. *Phys. Fluids*, **6,** Pt. 2, 962–972

Zilitinkevich, S., Grachev, A. and Hunt, J. C. R. 1998 Surface frictional processes and non-local heat/mass transfer in the shear-free convective boundary layer. In: *Buoyant convection in geophysical flows*. Eds. E. J. Plate, E. E. Fedorovich, D. X. Viegas and J. C. Wyngaard. Kluwer Academic Publishers, the Netherlands, 83–113

Zilitinkevich, S. S. and Esau, I. N. 2005 Resistance and heat transfer laws for stable and neutral planetary boundary layers: Old theory advanced and re-evaluated. *Q. J. R. Meteorol. Soc.*, **131,** 1863–1892

Zilitinkevich, S. S., Grachev, A. A. and Fairall, C. W. 2001 Scaling reasoning and field data on the sea-surface roughness lengths for scalars. *J. Atmos. Sci.*, **58,** 320–325

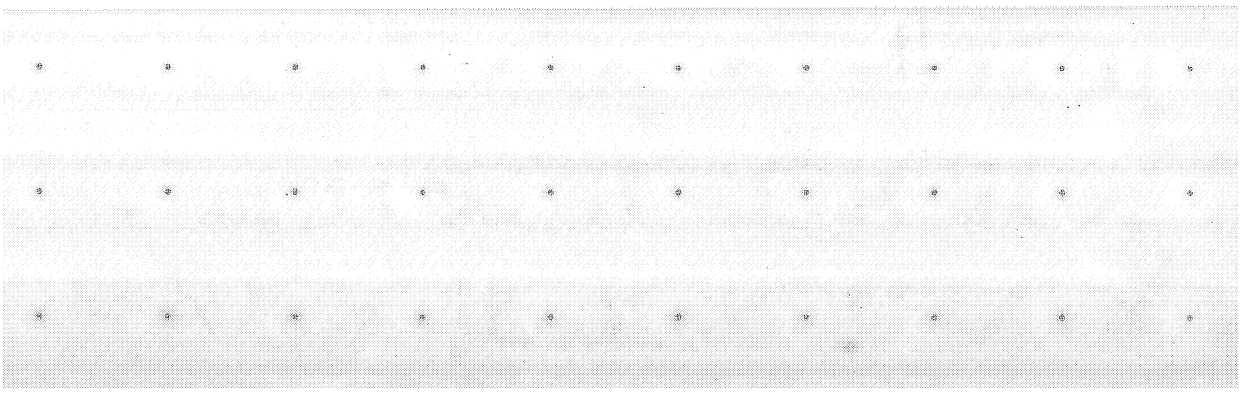

Zilitinkevich, S. S., Baklanov, A. and Joffre, S. 2003 'Effect of stratification on the surface resistance over very rough surfaces'. Subsection 3.2 in FUMAPEX Report 'Improved models for computing the roughness parameters of urban areas'. Eds. A. Baklanov and S. Joffre. DMI Sci. Report 03-19, ISB No. 87-7478-495-1, November 2003 (available from the Danish Meteorological Institute, Lyngbyvej 100, Copenhagen, Denmark)